Comprehensive review of the effects of ionizing radiations on the ZERODUR® glass ceramic

Antoine Carré,[a,*] Rule Kirchhoff,[a] Tony Hull,[b] Janina Krieg,[a] Daniela Eppers,[c] Marty Valente,[f] and Thomas Westerhoff[a]

[a]Schott AG, Advanced Optics, Mainz, Germany
[b]University of New Mexico, Albuquerque, New Mexico, United States
[c]Physikalisch-Technische Bundesanstalt, Braunschweig, Germany
[f]Arizona Optical Systems, Tucson, Arizona, United States

Abstract. The low thermal expansion glass ceramic ZERODUR® has a long and successful history in spaceborne optical applications. This material is especially used where precise shape invariance is required, i.e., for the mirror substrates dimensional stability when subject to temperature gradients and transients. In space, temperature may not be the exclusive driving force impacting the form stability; influence from ionizing radiations require considerations. The real impact of ionizing radiation on ZERODUR® has become a matter of reconciling, on the one hand, *in situ* experience, e.g., that the secondary mirror of low Earth orbit (LEO) Hubble Space Telescope crossing the South Atlantic Anomaly or the overall optics of geosynchronous equatorial orbit (GEO) Chandra X-ray Observatory are not reporting any specific problems related to dimensional stability at the optical form level. On the other hand, finite element simulation based on early lab experiments of ZERODUR® compaction are suggesting the opposite. This debate was brought to the forefront with the SILEX mission, where radiative ageing models were significantly overestimating the deformation experimentally observed on the lab replicas and were in even stronger disagreement with the observations collected over the mission. It has been speculated that an erroneous form factor in the physical model used to derive the phenomenological compaction law was responsible for these discrepancies. Following this hypothesis, we readdressed the effect of ionizing radiation induced by γ, electron, and proton fluences on ZERODUR® compaction. For each of these, we present and discuss the irradiation source, the experimental setup, the sample design, and the measurement procedure as well as the observations. Consistent with the feedback gathered over many different space missions, we confirm that the compaction observed is significantly smaller than the estimations available in the prior literature. © *The Authors. Published by SPIE under a Creative Commons Attribution 4.0 International License. Distribution or reproduction of this work in whole or in part requires full attribution of the original publication, including its DOI.* [DOI: 10.1117/1.JATIS.9.2.024005]

Keywords: optics; mirror; ZERODUR®; radiation; ionization; compaction; coefficient of thermal expansion; ageing; gamma; electron; photon.

Paper 23007G received Jan. 13, 2023; revised manuscript received Apr. 7, 2023; accepted for publication Apr. 10, 2023; published online May 3, 2023.

1 Introduction

For more than 50 years, the glass-ceramic ZERODUR®[1] has played an important role in design of stable mirror substrates and structures dedicated to astronomical applications.[2,3] For much of this period, ZERODUR® has also been successfully used in space. ZERODUR® is a lithium-aluminum-silica glass-ceramic, initially cast then annealed while remaining in an amorphous state. Next, a precise ceramization process enables the homogeneous distributed crystallization of a solid solution of eucryptite. Locally, this glass matrix has a net positive coefficient of thermal expansion (CTE), while the solid solution of eucryptite has a negative one.[4] Macroscopically the interplay between these two coexisting phases results in material having a net macroscopic CTE close to 0 ppm.K^{-1} over temperature range that may be centered on $T = 20$°C and spanning tens

*Address all correspondence to Antoine Carré, antoine.carre@schott.com

of degrees.[1] This supports form stability under thermal perturbations, but furthermore provides the critical features of high homogeneity, high isotropy and availability in large monolithic light-weigthed forms made of ZERODUR® the material of choice for sensitive telescope mirrors, typically in orbiting missions.[5,6] For these reasons ZERODUR® continues to be a widely employed material in space where high stability is needed. It is a critical part of more than 40 orbiting missions[2,3] among these two NASA great observatories, Hubble-M2 and all Wolter mirrors on Chandra.[2,3]

In spite of these successful applications, we note that the form stability of this material is not exclusively determined by its thermomechanical properties. Ionization due to space radiation should also be evaluated for possible impact on the optical figure.

A comprehensive understanding of the resilience of ZERODUR® under ionizing radiations is relevant to properly estimate the optical systems errors budget over the duration of the space mission. Mirror substrate materials can respond to local changes in their CTE induced by radiation. A CTE gradient, coupled with the temperature gradient, has the potential to drive local deformation of the optical surface depending of course on the susceptibility of the material properties to ionization.[7] Another effect of radiation induced change, namely compaction, may alter the surface form; here the deformations are not caused indirectly by local material shrinkage/dilatation under thermal load but are directly caused by the irradiation itself. The material shrinks under irradiation, i.e., its density (ρ) increases. The compaction effect $\Delta\rho/\rho$ can be quantitively defined as follows:

$$\frac{\Delta\rho(D)}{\rho} = -\frac{\rho(D) - \rho_0}{\rho_0}, \tag{1}$$

with $\rho_0 = \rho(D = 0)$ being the density of the material prior irradiation and $\rho = \rho(D)$ the density of the material after any given deposited total ionizing dose (TID) D. This effect has been extensively investigated for fused silica (see R.E. Schenker and W.G. Oldham[8] who gathered the different studies on this material[9–13]).

Quantifying the impact of ionizing radiation upon a specific spaceborne mission require extensive *a priori* information. Factors include mission duration, orbit, solar activity, as well as optical and telescope design (due to shielding) and orientation. All these parameters could drive to very different irradiation scenarios that obviously cannot be comprehensively addressed in a general discussion. A more general approach has been proposed by development groups[14–18] where a phenomenological law binds the deposited ionizing dose to the induced variation of material properties of interest. Coupled with finite element methods (FEMs) analysis these phenomenological laws offer much more flexibility in that the need for experimental testing on real size optics can then be to some extent circumvented via interpretation. One of the first phenomenological studies of ionizing radiations on ZERODUR® was initiated 40 years ago by Bourrieau and Romero.[15] This pioneering work proposed to estimate the indirect effect of ionizing radiation on the compaction by measuring the change induced in the vertex radius of curvature (VRoC) of flat discs. In this work, the compaction $\Delta\rho/\rho(D)$ was phenomenologically described by a power law of type: $\Delta\rho/\rho(D) = A \times \sqrt{D}$. This contribution is laudable, but the lack of computational power in that time constrained the authors to coarsely approximate the irradiated ZERODUR® discs into a bimetallic system. The continuous gradient of deposited ionizing dose through the thickness of the coupon was approximated by a heavyside function (whose step position corresponds to the relaxed solarized/unsolarized interface within the glass ceramic). In this model, the radial distribution was neglected and the coupons were assumed to be thin plates (radius $>10\times$ thickness). The authors derived the compaction law using the Timoschenko bimetallic approach[19] on this ideal 1D approximation. However, this compaction law has been challenged some years after by Higby et al.,[16] who used a more conventional but less sensitive approach where coupons of ZERODUR® have been irradiated and the shrinkage has been estimated by densimetry. The compaction law proposed by this research group was in disagreement with the one proposed by Bourrieau and Romero.[15] A third contribution weakened further the phenomenological compaction law proposed by Bourrieau and Romero.[15] During the preparatory phase of the ESA's Artemis mission, a consortium made of the ESA/ZEISS/ONERA/SCHOTT was able to cross-validate neither the experimental results observed on the SILEX mirror replica nor the numerical multilayer modeling based on the Bourrieau compaction law.[15] The computed

defocus contributions attributed to compaction were found to be significantly higher than the experimental ones. These inconsistencies drove Davis and Fainberg[14] to reassess the compaction law initially proposed by Bourrieau.[15] In their methodological contribution, these authors suggest that a form factor in the bimetallic equation could be erroneous (5× to 10×) and cause a systematic overestimation of the compaction. Interestingly, all the experimental efforts made in order to derive an empirical compaction law[20] were made at the beginning of the 1980s during the US/Soviet Union missile race; thus, these research efforts were mostly addressing potential consequences of weapons effects rather than environmental impact on spaceborne telescope or optical assembly. This context explains why the levels of radiation considered in these publications were very high compared to most space natural environments achieved and those measurements involved using a high flux of particles heating coupons (up to 70°C[16]). In addition, measurements were made considering that a nuclear blast rich in soft x-rays absorbed in the mirror's shallow level, often were sufficient to cause surface spalling.

Review of the technical contributions over the past four decades exposes the need to refine the understanding on the compaction law as applied to spaceborne mirrors. This is the aim of the present contribution.[21] Here we derive compaction laws using both the densimetric approach (the experimental observable is the density) and the interferometric approach (the experimental observable is then the deformation of the optical substrate, i.e., closer to a real case in orbit). These two approaches are very different in their concept and can be viewed as being complementary. Neither is suited for all types of ionizing radiations. Densimetry can be more reliably measured on homogeneously irradiated coupons, ideally large coupons (about 1000 g), while interferometry is more adapted to very heterogeneous dose distributions and can be applied to small coupons. Densimetry is more adapted to where the ionizing particle has a large penetration depth, contrary to situations where interferometry is employed. Densimetry will give direct access to the compaction law whereas interferometry will require more physical insight in order to derive a compaction law. The definition of a compaction law implicitly assumes a definition of the deposited dose into the Device Under Test (DUT), here into the ZERODUR® coupons. Each of the experimental setups for γ, e^-, and H^+ has been modeled using Geant4[22,23] version 10.03p03 using the standard EM package for the description of the physics interaction processes. This simulation toolkit is also embedded in the internet interface SPENVIS supported by the ESA[24] for modeling the space environment (e.g., cosmic rays, natural radiation belts, etc.) and its effects.[24] These dose(-rate)-depth profiles once simulated via Monte-Carlo methods, give a quantitative estimate of the deposited dose equivalent to those provided by SPENVIS tool[24] (for example MULASSIS or GRACE) on ZERODUR®.

We observe that the ionizing particle energy spectra over low Earth orbit (LEO)/geosynchronous equatorial orbit (GEO) is dominated by low-energy particles having a small penetration depth. Therefore, the resulting TID-depth profile has dose asymptotically decreasing with depth. In the space environments considered, deposited ionizing dose may span several orders of magnitude over a depth of few micrometers. As a practical matter, any design of experiment (DOE) addressing the ageing behavior under space ionizing radiation should explicitly cover this range of magnitude. Later, we discuss the effect of monoenergetic laboratory generated dose-depth profiles, which are several orders of magnitude larger than typical dose-depth profile expected on orbit. As mentioned, the experiments presented here do not define any specific concept of operations (CONOPS), our results serve the purpose of fitting a phenomenological compaction law that can then be used to estimate the resilience of ZERODUR® over the targeted mission.

In the following sections, we will present the different types of radiation used to characterize the compaction law(s), first introducing the method and then the results collected with γ, electron, and proton particles. Next, we introduce the mathematical and physical approaches used to derive compactions laws related to the different types of particles. The significance of these results is discussed.

2 Experimental Results

All the experiments summarized here are designed to define compaction laws describing the response of ZERODUR®. Since these results cannot be directly applied to a specific CONOPS at this time, we summarize these differentiators in Table 1 below.

Table 1 The contrast between the space and laboratory irradiations is summarized. Spaceborne conditions are from the AP8 and AE8 Max estimates made using a METEOSAT10 GEO orbit computed with SPENVIS[24] using the AE-8 and AP-8 particle distribution models.

				Typical flux	
Particle	Env.	Angular distribution	Energy distribution	Energy (MeV)	Flux ($cm^{-2}.s^{-1}$)
e^-	Space	Omnidirectional	Continuous	>1.0	$[10^4; 10^7]$
e^-	Lab	Point source, normally distributed	Monoenergetic	1.5	1×10^{11}
H^+	Space	Omnidirectional	Continuous	>1.0	$[10; 10^7]$
H^+	Lab	Collimated	Monoenergetic	23.0	$1 \times 10^{10} - 1 \times 10^{11}$

The irradiation scenario timescale between the laboratory and the space conditions obviously is very different, and it is impractical to continuously irradiate coupons over a decade because of cost and irradiation stability considerations. These accelerated particle fluxes potentially could introduce two main experimental biases. First, the energy imparted in the target by accelerated fluence of the ionizing particles is converted into heat, and any overheating of the samples, even on a microscopic scale, may lead to unwanted thermally activated healing and induce additional failures that would not have occurred under much more moderate environmental fluences. Large fluxes may induce instantaneously large defect concentrations that may eventually heal and relax over an extended time scale, implying the effects observed directly after irradiation may be misleading, as they do not represent the steady state. To mitigate the contribution of these two effects on the characterization of the resilience of ZERODUR®, we performed all irradiation experiments under controlled temperature (samples were maintained at room temperature). Moreover when possible, we characterized the impact of irradiation for up to a 1-year time span. Discrepancies in the damaging/healing kinetic of ZERODUR® and characterization of steady-state fluence have already been investigated on ZERODUR® by Doyle et al.[25] In this work, the authors observed similar coupons in deformation under two very distinct β-irradiation levels, by means of Sr90-Y90 decay and a Van de Graaf accelerator (100× temporal acceleration).

In all following subsections, the local deposited TID (D) within the sample can formally be approximated

$$D(x, y, z, t; E_{\text{particle}}) = \frac{dE}{dm}(x, y, z, t; E_{\text{particle}}) = \frac{1}{\rho S}\frac{dE}{dz}(x, y, z, t; E_{\text{particle}}), \tag{2}$$

with:

- x, y being the position of the volume element on the plane normal to the direction of the incident ionizing particles;
- z being the depth of the elementary unit of material considered;
- t the duration of the exposure;
- E_{particle} the energy of the incident ionizing particle;
- dE the elementary amount of ionizing energy deposited;
- dm the elementary mass considered, presently ZERODUR® ;
- ρ the material density, presently ZERODUR®;
- And S the surface area being irradiated;

The amount of energy deposited is directly proportional to the fluence of ionizing particle fired onto the target. Maintaining the experimental setup constant over the irradiation time, we vary only the fluence of particle being fired onto the target ($n(t)$) yielding:

$$E(x, y, z, t; E_{\text{particle}}) = e(x, y, z; E_{\text{particle}}) * n(t), \tag{3}$$

Table 2 Irradiation and measurement procedure used for the investigation of the compaction. Some well characterized commercial charges have been selected to manufacture these samples, namely Charge H12132 Article No. 1010088 having a CTE $= -0.004$ ppm.K^{-1} and I10414 Article No. 1066717 with a CTE $= 0.021$ ppm.K^{-1}, both charges belonging to the expansion class 0 and having a standard striae, inclusion, and bubble level.

Particle	ZERODUR® charge	Geometry (mm)	Surface quality	Coating	Measure	Dose range (Gy)
γ	H12132	$\phi 90 \times 62.3$ mm	P3 (P1-P2 for edge polishing)	No	Densimetry	1×10^5
e^-	I10414	$\phi 50 \times 5$ mm	P3 (optical surface) – remaining surface acid etched	Yes (Al 120 nm)	Interferometry	$1 \times 10^3 - 1 \times 10^6$
H^+	I10414	$\phi 50 \times 5$ mm	P3	No	Interferometry	$3 \times 10^4 - 1 \times 10^7$

with $e(x, y, z; E_{\text{particle}})$ being the average ionizing energy imparted in the system per fired incident ionizing particles and consequently

$$D(z, t; E_{\text{particle}}) = \frac{1}{\rho S}\frac{dE}{dz}(z, t; E_{\text{particle}}) = \frac{1}{\rho}\frac{de(x, y, z; E_{\text{particle}})}{dz}\int_{u=t_0}^{u=t}\frac{1}{S}\frac{dn(u)}{du}\mathrm{d}u. \tag{4}$$

In the above equation, $\frac{1}{S}\frac{dn(t)}{dt}$ represents the particle flux in number of particles being fired per second and per unit of surface, and $\int_{u=t_0}^{u=t}\frac{1}{S}\frac{dn(u)}{dt}\mathrm{d}u$ corresponds to the particle fluence over the temporal range $[t_0; t]$. In the subsequent sections, namely for γ, $e-$, and $H+$ irradiations, we systematically kept the experimental setups constant (positioning, particle energy, i.e., the deposited energy distribution profile $e(x, y, z, E_{\text{particle}})$ was constant) and we only modulated (decadic) the fluence either by changing the duration of the coupon exposure t or via the particle flux $\frac{dn}{du}$; the shape of the dose profile within the DUT remained unchanged over the given ionizing experiment.

In the following subsections γ, $e-$, and $H+$ irradiations are introduced according to the experimental chronological order, α, $e-$, and $H+$, respectively. The $e-$ and $H+$ irradiation experiments are based on the same measurement principle. However, the observations made during electron irradiation showed that we could loosen the specifications regarding the manufacturing of the H^+ coupons without impairing significantly the quality of the results. A short overview of the samples design considered in the following subsections is provided on Table 2.

2.1 *Gamma Irradiation*

Gamma radiation is routinely considered when dealing with material or component resilience in space. The large penetration depth of gamma particles enables the direct characterization of the compaction by means of densimetry, thus large samples provide better results. First, DOE methods have been used to define the electron and proton irradiation experiments.

2.1.1 *Irradiation configuration*

The γ irradiation experiments presented here have been achieved using the radio-isotope of Cobalt, ^{60}Co. The decay of ^{60}Co into ^{60}Ni is associated with emission of two γ photons having energies of 1.17 and 1.33 MeV. These high-energy particles interact with the electronic structure of the mirror material and generate electronic defects (ionization) as well as secondary electrons via three main mechanisms

- photoelectric effect;
- Compton scattering;
- and marginally, pair production.

These irradiation experiments have been conducted at the ^{60}Co facility of the ESTEC. The ESTEC ^{60}Co facility is accredited by RvA (Dutch Accreditation Council) according to ISO/IEC 17025.2005(L517) for methods to accurately determine TID and Dose Rate.

The ZERODUR® coupons have been embedded in ZERODUR® material surrounds and placed at a distance of $l = 400$ mm from the γ source. The dose rate in water is measured at this position by means of a PTW TW30012-10 ionization chamber giving a value of $\dot{D}_{\text{water}} = 112.5$ Gy.h^{-1} (the uncertainty budget is 4.4% with k = 2 for absorbed dose rate in water, i.e., ± 4.5 Gy.h^{-1}).

Six coupons have been irradiated with this setup, all with different exposure times. All exposure times are approximate and integer multiples of each other. However, the overall duration of the experiment was limited by the irradiation facility available time, and because of this, it was not possible to repeat some experimental points. As a first approximation, the attenuation of electromagnetic radiation in the material is expected to follow a Lambert's law[26] $\propto e^{-(\frac{\mu}{\rho})\rho x}$, consequently the dose deposited in the cylindrical coupon exhibits a similar decreasing exponential profile along the coupon rotation axis. This profile is characterized by the total mass attenuation coefficient $\frac{\mu}{\rho}$ whose value has been estimated by measuring experimentally the dose in water behind ZERODUR® coupons exhibiting different thicknesses, thus determining $\frac{\mu}{\rho} = 0.0562$ cm^2.g^{-1} for $E = 1.25$ MeV. With this estimate of the mass attenuation coefficient, we can reasonably approximate the dose profile as linearly decreasing profile over the length of the DUT, $e^{-(\frac{\mu}{\rho})\rho x} \simeq 1 - \mu x$. To mitigate the axial changes introduced by the dose gradient, the coupons have been turned around after one half of the total irradiation time. The cumulated dose in water has been measured directly at the back of the assembly (coupon + build-up material) during the first half of the irradiation (see Fig. 1), and then again after the duration of the second half of the irradiation. This duration has been corrected so that the cumulated dose in water measured matches after the second half that measured during the first half. By doing so, we also compensated for the marginal decrease of activity of the ^{60}Co source over the irradiation time.

The temperature of the irradiation facility has been kept constant around $T = 22.4$°C $\pm$ 0.2°C over the duration of the irradiation.

2.1.2 *Coupons design*

Since the ^{60}Co is implemented as an isotropic emitting point source, the irradiation field in the plane normal to the ^{60}Co source axis is then axisymmetric.[27] To take full advantage of this feature we designed cylindrical pieces of ZERODUR®. Beyond this irradiation constraint, we also had metrology constraints that drove this geometrical approach. The density of the coupons is measured at Physikalisch-Technische Bundesanstalt (PTB) using a specific hydrostatic balance. High measurement precision requires that the coupons fulfill prerequisites: The weight of each coupon must be within the [1000; 1005] g range, since this range corresponds to the tight

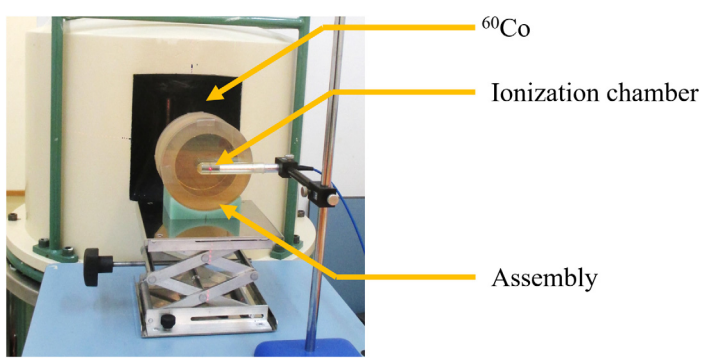

Fig. 1 Picture of the DUT (ZERODUR® cylinder embedded into the ZERODUR® surround material) is placed in front of the ^{60}Co source. The absorbed dose monitoring is achieved by means of a ionization chamber placed at the back of the DUT.

calibration range of the scale. The symmetry and weight constraints, combined with demand for high fluence (i.e., compactness of the irradiated cross section close to the ^{60}Co source), resulted in design freeze with $\varnothing = 90$ and thickness $=62.3$ mm (the individual thicknesses of the coupons have been controlled and adjusted to meet the weight requirement). The hydrostatic metrology principle involves immersion of the coupon. The measurement can be impacted if wetting of the glass into the immersion oil is imperfect, since then the presence of air cavities would bias the measurement. Tests made on ZERODUR® coupons having different level of ISO10110 polishing quality P1, P2, and P3, showed that a quality of P2 or higher was required to ensure the required surface wetting and to avoid air cavities. Practically the coupons have been polished to a P3 surface quality level for the front and back faces, P2 for the sidewall, and technically it was only possible to achieve a P1 quality for the chamfers of the coupons. However the smallness of the chamfered area made its contribution negligible ($\leq$1% of the overall of the ZERODUR® coupon area).

Irradiation by means of γ particles is associated with the build-up effect, with the maximum dose deposited a few millimeters deep in the material. To minimize the impact of this dose-deposition gradient, we manufactured a surround structure/holder also made of ZERODUR® that tighlty encases the DUT coupons. This is implemented to promote the Compton scattering equilibrium (see Fig. 2) and is believed to entirely mitigate Compton scattering variance on the coupon to the accuracy of the experiment.

The surround consists of a large cylindrical ring, as mentionned made of ZERODUR®, that tightly fits around the DUT diameter. Additionally, the DUT is surrounded front and back by disks of ZERODUR®. The contact surfaces between the build-up structure and the DUT have all been polished to avoid scratches (and associated later air cavities).

2.1.3 *Measure*

Density measurements of solids are carried out with an automatically operating measuring apparatus at PTB.[28] The measurements have been all performed in a thermally stable environment with a temperature $T = 20.02°\text{C} \pm 0.01°\text{C}$. The density is obtained by determining the mass and the volume, whereby the mass is measured by comparison with mass standards and the volume is measured by hydrostatic weighing, see Fig. 3. The mass of the coupon is determined by differential weighing using the substitution method, in which the mass standard and the solid coupon are compared successively on the same weighing pan of a high-resolution mass comparator. The masses to be determined are traceable to the SI base unit kilogram. Hydrostatic weighing is a metrology method that determines the density or volume of solids by measuring the buoyant force acting on a solid in a liquid. This method follows from Archimedes' principle, which states that a fully immersed solid appears to lose as much weight as the amount of liquid displaced.

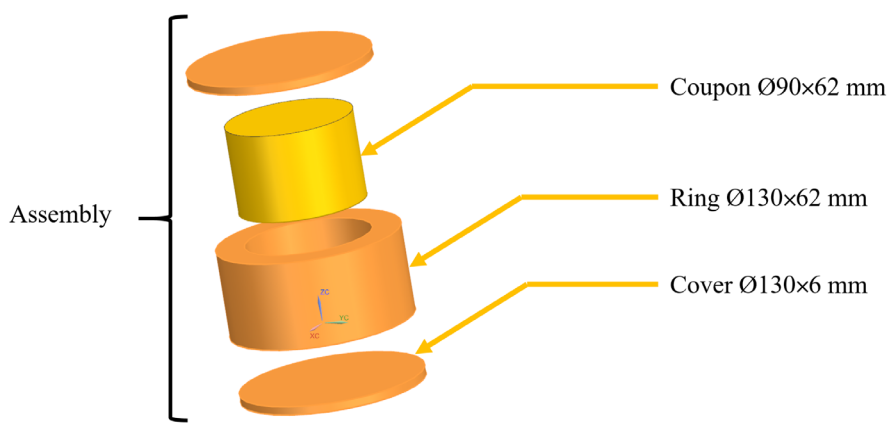

Fig. 2 Sketch representing the surround assembly implemented for γ irradiation of ZERODUR®. The ZERODUR® DUT (yellow) is embedded into ZERODUR® surround material (orange).

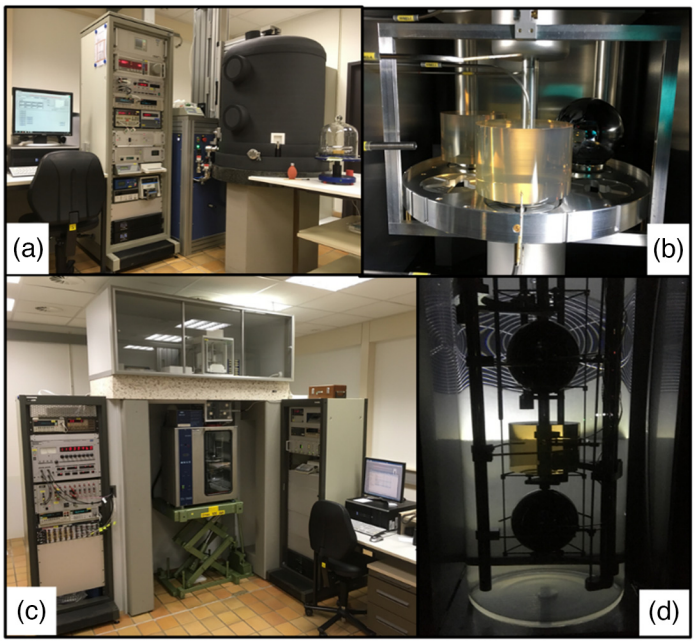

Fig. 3 (a) The cloche protecting the mass comparator from thermal noise and convective flow. (b) ZERODUR® coupon in the weighing basket. (c) Overview of the hydrostatic weighing scale. (d) Closer view if the hydrostatic scale with a ZERODUR® coupon located in the middle basket - below and above Si density standard used for determining the actual density of the immersion fluid.

Thus, by means of the apparent weight loss or buoyancy $\rho_l V g$ (liquid density ρ_l, volume of the solid V, and local gravitational field of earth g), the density or volume of a solid coupon can be determined. For this purpose, the solid DUT is placed between two density standards (1 kg spheres of natural silicon) of known density and volume in an organic metrology liquid (here n-pentadecane $C_{15}H_{32}$, $\rho \simeq 769$ kg.m^{-3} at 20°C). The two density standards and the solid coupon are weighed alternately with a mass comparator. The solids are deposited via a suspension gear at different heights, connected to the balance by a wire. An exchange mechanism for hydrostatic weighing allows the solids to be weighed independently by placing on and removing the solids from the suspension gear. The two density standards are used to determine the liquid density. The liquid density at the position of the coupon can be obtained by interpolating the liquid density of the position of the density standards to the position of the coupon. With the calculated liquid density, the density or volume of the coupon can be determined by taking into account the buoyancy force and the weight reading. To achieve small measurement uncertainties, a mass comparator with a measuring range of 1 kg and a resolution of 1 μg is used. For this purpose, the weight readings must be adjusted to the measuring range of the mass comparator. An automatic handler in the balance is used to place additional standards (stainless steel weights) on the weighing pan, the weight of which is added to the weights of the coupon or the density standards. If the coupon and standards are very similar in mass and volume, the highest accuracy is obtained when the apparent weights of the coupon and standard are compared in both liquid and air and only the differences are measured. In this way, the densities (and volumes) of the coupons of ZERODUR® ($V = 396.3$ cm^3) studied here can be compared with an uncertainty for the density of $\rho = 0.0022$ kg m^{-3}, i.e., 2 ppm ($k = 2$).

To investigate both potential drift over the metrological chain as well as any external effect that could have induced a density change we purposely kept a reference coupon unirradiated throughout the experimental process. This coupon testifies the absence of changes induced by environmental parameters over the duration experiments. This demonstrates a density metrology drift not greater than 0.0004 kg.m^3. The average density of all six samples prior to irradiation has been determined being $\rho = 2534.0425$ kg.m^{-3}.[29]

2.1.4 *Simulation*

Our experimental setup has been simulated using the Geant4 software package.[22,23] The ^{60}Co source has been approximated[27] as a point source located at 400 mm from the target, while the surrounding space is regarded to be made exclusively of air. To reduce computational time we have made a reasonable approximation of only considering the γ particles whose initial direction crosses the target (the target corresponding to a solid angle Ω_{Cylinder}). The density of particles fired per unit of solid angle has been set constant for the simulation. Here, the simulated target is a cylinder representing both the assembly coupon and surround, i.e., a $\varnothing = 130$ mm, height 75-mm cylinder of ZERODUR®. The γ particles energy distribution is represented by two Dirac delta functions centered on 1.17 and 1.33 MeV. For this purpose ZERODUR® has been defined using the individual National Institute of Standards and Technology (NIST) element definition set and weighting by the ZERODUR® composition,[1] and the density has been set to $\rho = 2.53$ g.cm^{-3}.[1] The number of particles N fired onto the target over the simulation can be summed into a duration Δt following:

$$\Delta t \simeq \frac{1}{a\mathcal{A}}\left(\frac{4\pi}{\Omega_{\text{Cylinder}}}\right)\left(\frac{N}{2}\right), \tag{5}$$

where activity $\mathcal{A}$ corresponds to the activity of the source at the time considered and a being the source self absorption coefficient.[30] This equation assumes that the overall activity $\mathcal{A}$ does not decay significantly over the duration of the irradiation experiment $\frac{\Delta t}{\mathcal{A}}\frac{\partial \mathcal{A}}{\partial t} < 1$, i.e., experiments lasted about 1 month, to be compared with a half-life of ^{60}Co of 5 years. The local dose rate can then be expressed as being the deposited dose per volume element over the simulation divided by the exposure time. Due to this simplification, the contribution of particles scattered by the surrounding environment is not taken into account (back-scattered particles on irradiation facility, table, mount, etc.) and is believed negligible. The corresponding computed dose-depth profile is represented on Fig. 4. Based on this profile, the average TID-rate in ZERODUR® has been estimated being about 68 Gy.h^{-1} (see Fig. 4 horizontal dashed line).

The computed dose-depth profile of water has also been added to Fig. 4, the simulated value read at the charged particle equilibrium (CPE) in water is 107 Gy.h^{-1} in reasonable agreement

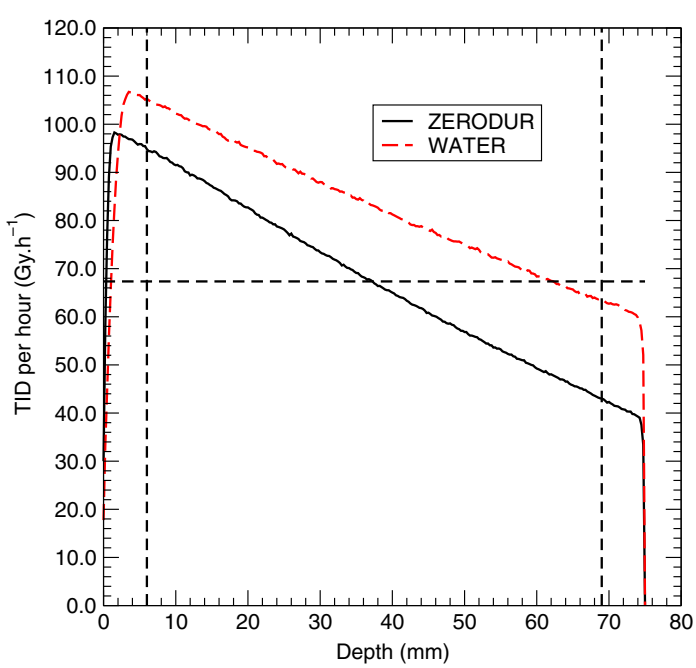

Fig. 4 Dose-depth (TID) rate calculated using Geant4 on the ZERODUR® cylinder. The two vertical lines represents the limit of the shielded domain (build-up material). The horizontal line corresponds to the estimated average TID (mean of a function) within the ZERODUR® DUT.

with the experimental measure achieve with the PTW TW30012-10 ionization chamber, 112.5 Gy.h^{-1}, i.e., about 5% mismatch between the simulation and the measure.

We also used the mass-attenuation coefficient to provide an estimate of expected dose in ZERODUR®. To this end, we need to rescale the dose in water as read with the ionization chamber. This has been accomplished by referencing the tabulated experimental mass energy absorption coefficient of a well-calibrated material like Borosilicate glass (similar to ZERODUR® in term of density, SiO_2 and alkali contents) divided by the corresponding experimental coefficient of water at an energy of 1.25 MeV available in the NIST database,[31] $\frac{\frac{\mu_{en}}{\rho}|_{glass}}{\frac{\mu_{en}}{\rho}|_{water}} = \frac{2.650*1\times10^{-2}}{2.9655*1\times10^{-2}} = 0.8937$. Thus, we can propose an estimate of the dose rate in glass under conditions of secondary CPE by about 98 Gy.min^{-1}, also in qualitative agreement within 14% to the calculated CPE TID dose rate in ZERODUR® presented on Fig. 4.

Based on those value, we estimated the overall uncertainty budget (measure + simulation) for the TID dose in ZERODUR® about 20%.

2.1.5 *Results*

The graphical representation of these density variations[29] as a function of both the particle fluence and the estimated average deposited TID is provided on Fig. 5. The variation of density for 10 and 100 Gy exhibit large uncertainties. Above 100 Gy, the linear aspect of the compaction data in Fig. 5 strongly suggests that the phenomenological law binding the ionizing dose to the compaction can be optimally described by a power law.

2.2 *Electron Irradiation*

For required precision, densimetry requires large coupons ($m \simeq 1000$ g, i.e., typically $(m/\rho_{\text{ZERODUR}})^{1/3} \simeq 75$ mm large coupons). While not possible to homogeneously irradiate such

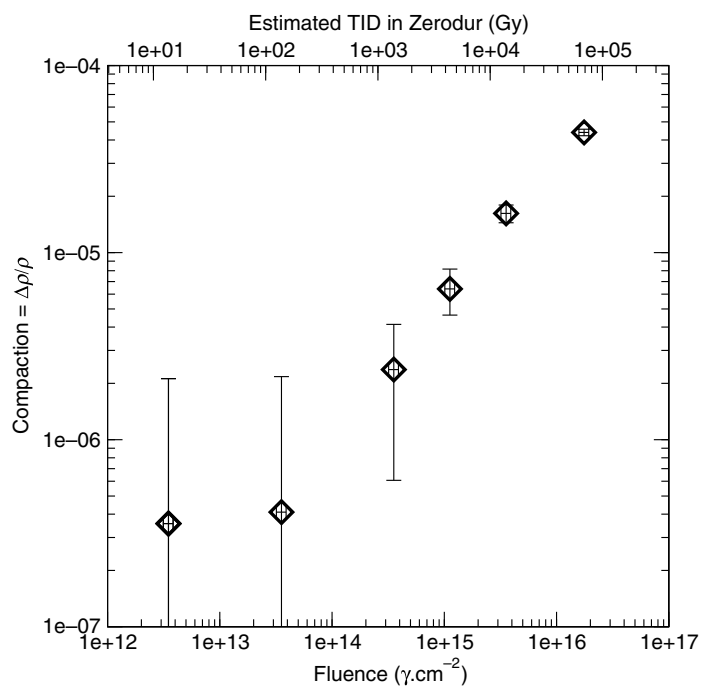

Fig. 5 Compaction of ZERODUR® as a function of the γ fluence (bottom abscissa) and corresponding estimated TID (top abscissa) achieved by means of ^{60}Co. The fluence ϕ of primary γ particles has been calculated $\Phi = \mathcal{A} a \frac{\Omega}{4\pi} \frac{1}{\pi r^2} \Delta t$, with $\Omega \simeq \pi(\frac{r}{l})^2$ being the solid angle of the coupon (radius $r = 45$ mm) seen from the source (distance $l = 400$ mm), $\mathcal{A}$ the source activity ($\mathcal{A} = 58.5$ TBq at the time of the irradiation and a the source self absorption coefficient of $a = 0.8352$.[30]

large coupon with electrons without massively activating the coupons (activation energy threshold ≥10 MeV), nevertheless, the effect compaction can still be indirectly determined by measuring the bending of superficially irradiated discs, as originally proposed by Bourrieau et al.[15] This approach can easily be achieved using ≃1 MeV incident kinetic energy electrons followed by ultraprecise measurement of radiation induced coupon curvature. While the curvature comprises mostly optical power, this directly relates to the expectation of optical surface error over a spaceborne telescope's mission.

2.2.1 *Irradiation configuration*

Irradiation has been performed at the research linear accelerator of the Metrological Electron Accelerator Facility of the PTB.[32,33] The energy of the electrons used for the irradiation was 1.5 MeV. This energy corresponds to a technical compromise; ideally, lower kinetic energy electrons (≤1.5 MeV) are preferable since they better mimic the space environment. However, the penetration depth of lower-energy electrons is also lower, and the expected effect on the coupon bending is then more complex to resolve. At lower energy, the electrons are also more easily scattered by the surrounding environment. Thus, the electron flux is also more difficult to monitor. For these two reasons, we selected a 1.5 MeV e^- incident energy to characterize the compaction effect. The electron beam is pulsed with a typical pulse width of 2.5 μs. The pulse repetition frequency used during the irradiation was 50 Hz. An integrating current transformer (ICT, Bergoz Instrumentation) is installed at the end of the accelerator beamline for non-destructive charge measurement of the electron pulses for beam monitoring. At the end of the accelerator beam line the collimated electron beam passes through a 0.05-mm-thick titanium foil vacuum window which scatters the beam. The diameter of this window is much larger than of the beam, thus all electrons detected by the ICT have been contributed to the radiation field. The scattering in the titanium foil yields an electron radiation field with a normal radial distribution. The width (equivalently the standard deviation σ) of the field distribution increases with decreasing energy and increasing distance to the source. The width of the lateral dose distribution as function of the distance was determined experimentally by means of a Kodak ACR 2000i computed radiography system equipped with 240×300 mm^2 storage plates. The coupons were irradiated on the central axis of the radiation field at a distance of 250 mm measured by a laser distance measuring sensor, (see Fig. 6). At this distance the width of the field is considered to be

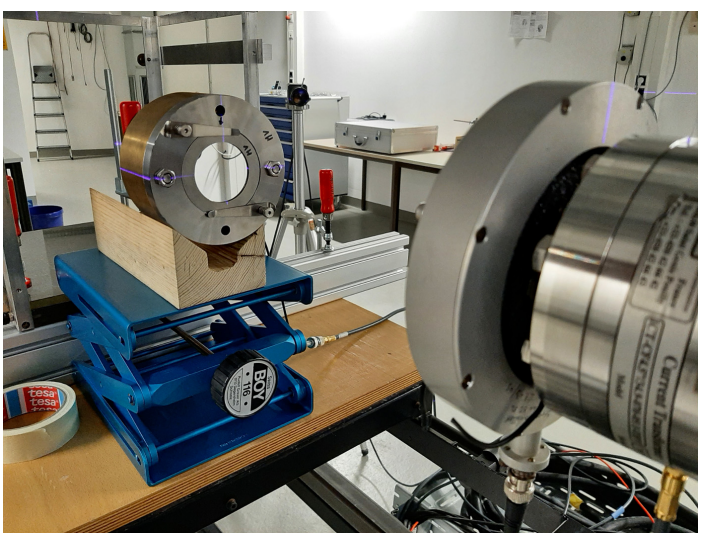

Fig. 6 Coated ZERODUR® coupon mounted on the aluminum holder. During the experiments two identical aluminum holders have been used to ease the coupon swappingexchange. The aluminum holder is fixed on a bronze block connected to a current integrator. The cumulated charge measured was used to quantify the amount of e− fired onto the DUT. The ensemble ZERODUR® + aluminum mount + bronze was resting on a wood block to electrically isolate the system and avoid biasing the measure. The coupon was centered and positioned at 250 mm from the beam line exit.

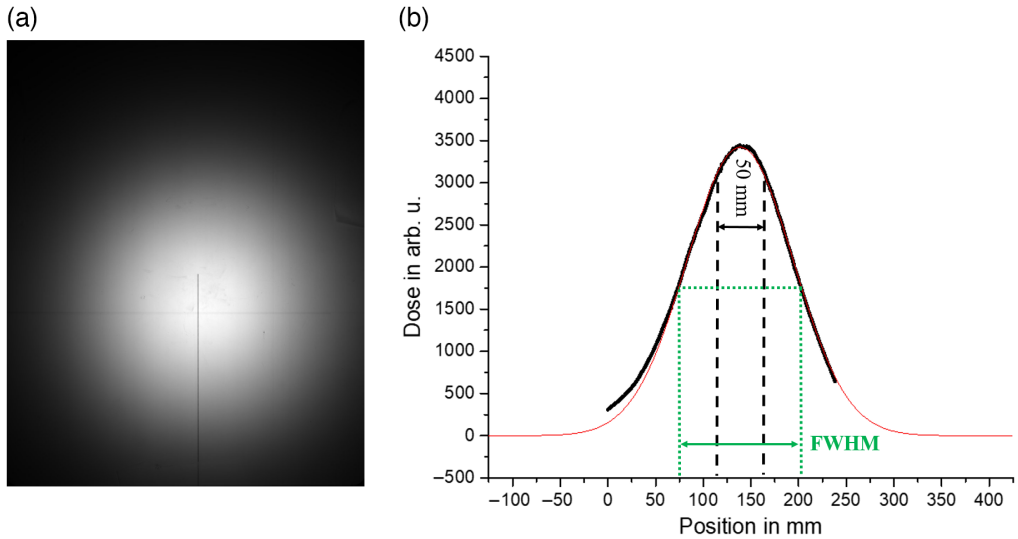

Fig. 7 Distribution of the local deposited dose. (a) Irradiation pattern printed on a photostimulable phosphor (PSP) plate as part of a Kodak ACR-20001 computed radiography system. (b) Corresponding experimentally measured radial intensity in red value and in black, the normal fit based on these experimental $dP(r,\theta) = f(r,\theta)\mathrm{d}r\,\mathrm{d}\theta = \frac{1}{\sigma\sqrt{2\pi}} e^{-\frac{1}{2}\left(\frac{r}{\sigma}\right)^2} r\mathrm{d}r\,\mathrm{d}\theta$, with $\sigma = 58.3 \pm 2.4$ mm, i.e., FWHM of FWHM $\simeq 2.355\sigma = 137$ mm. The dimension and centering of the coupons is represented by the two vertical black dashed lines.

sufficiently large (experimentally $\sigma = 58.3 \pm 2.4$ mm for a 1.5 MeV electron beam, see Fig. 7) to achieve homogenous or uniform irradiation, i.e., a dose variation is not larger than

$$\int^{u=r} e^{-\frac{1}{2}\left(\frac{u}{\sigma}\right)^2} u\mathrm{d}u = 1 - e^{-\frac{1}{2}\left(\frac{r}{\sigma}\right)^2} = 90\%, \tag{6}$$

over the surface of coupon to be irradiated.

The quantity of electrons fired onto the target is estimated by multiplying the charge per pulse measured by the ICT by the fraction f of electrons collected on the circular cross section $r = 25$ mm. The fraction f is defined by means of its radial Gaussian distribution, $f = 1 - e^{\frac{1}{2}\left(\frac{r}{\sigma}\right)^2}$. The uncertainty regarding this factor $\delta f/f$ can be linked to the uncertainty in the determination of the Gaussian parameter σ

$$\frac{\delta f}{f} = \frac{1}{f}\left(\frac{\partial f}{\partial \sigma}\right)\Delta\sigma = \left(\frac{r^2}{\sigma^3}\right)\frac{(1-f)}{f}\Delta\sigma. \tag{7}$$

The uncertainty estimated for $\delta f/f = 8\%$ for $\Delta\sigma = 2.4$ mm.

For validation reasons the irradiations have been indirectly monitored using the cumulated charge collected on the metallic coupon holder. In this manner, we determined in the linear correlation relating the charge monitored with the ICT to the charge collected on the coupon mount. The charge collected on the mount (acting as a Faraday cup in this context) is slightly higher than the estimated charge of primary electron being fired onto the DUT. This discrepancy is attributed to the contribution of secondary electrons. $q_{\mathrm{FC}}/q_{\mathrm{ICT}} \simeq 0.5951$, whereas $q_{\mathrm{DUT+mount}}/q_{\mathrm{ICT}} \simeq 0.411$. This factor has been measured with a relative uncertainty of 0.2%. Irradiation has been performed with this setup for different durations in order to generate an estimated maximal local TID deposition of 10^3, 10^4, 10^5, and 10^6 Gy, respectively, in the discs (see Sec. 2.2.4). The different dose depth profiles (only differing by their amplitude) have been generated by varying only the duration of the exposure over four orders of magnitude.

The irradiation procedure has been repeated to gain statistical confidence, however, for practical reasons it has not been possible to equally repeat all the irradiations (in total we performed 2×10^6 Gy, 8×10^5 Gy, 7×10^4 Gy, and 5×10^4 Gy irradiations for a total of 23 coupons).

The temperature generated by the electron flux within the samples has been periodically monitored and was systematically below $T = 25°C$ (measured at the center of the sample, i.e., were the local e− flux is maximum), even after a long exposure (corresponding to the targeted 10^6 Gy peak). Thus, temperature rise is irrelevant to our result. To be able to detect *a posteriori* any possible beam drift and misalignment all the samples had a specific clocking during irradiations, the same clocking mark was used for the before and after interferometric measurements.

2.2.2 *Coupon design*

The discs geometry is defined by three main constraints. First, the effect of irradiations should be sufficient to induce a measurable deformation. This implies that the penetration depth of the electrons (determined by their energy) should be about one half of the coupon thickness in order to behave in a similar manner as a bimetallic structure. If the coupons are too thin, then the compaction gradient will be too flat, and the bending of the coupons would be too weak for precise measurement. On the other hand, thick coupons (i.e., thickness significantly larger than e^- penetration depth) will minimally bend due to the overall stiffness of the unirradiated domain and thus have a low signal-to-noise level in interferometry. Preliminary dose-depth estimation performed using Geant4, suggested that e^- particles having an incident kinetic energy of $E =$ 1.5 MeV should induce a dose-depth profile over the first 2.5 mm of the coupon thickness. The coupon radius(r) should also not be small. According to the thin plate model, the VRoC R induced by irradiation should be independent from the sample radius. However, the sagitta or the PV error (in the case of pure spherical deformation) both scale like the square of the coupon radius ($\propto r^2/R$). Sagitta or PV error must be measurable by an interferometer, so the geometry of the specimens must be appropriate to this last requirement.

A large coupon radius implies that the coupons must be distant from the e^- beam to maintain a relative homogeneity of the irradiated area. Large irradiation distances are correlated with lower particle flux and longer irradiation time. The duration of the irradiation is also an important factor, since this drives the costs and is also limited by the beam stability and/or the availability of the particle beam.

After evaluating the different possible scenarios (supported by the results of the γ irradiation), it was decided to manufacture $\varnothing = 50$ mm thickness = 5 mm coupons to perform this DOE (see Fig. 8). The coupons have been polished by an optical flat manufacturer (Sydor Optics) using their standard double-side polishing processes to satisfy a requirement of <100 nm root-mean-square (RMS) surface figure error. At this level, precise interferometry at the nanometer level is feasible. One surface on each of the coupons was flash coated with bare aluminum. The coating was applied at room temperature and the thickness is 120 nm ($-0/+100$ nm). The uniformity of the layer is <1 nm across each part. The coating has two functions.

- Help the conduction and the flushing of electrons from the surface through the mount to the current integrator, therefore potentially avoiding damages due electrical breakdown. Here we observed experimentally that the charge collected onto an Al coated coupon versus bare

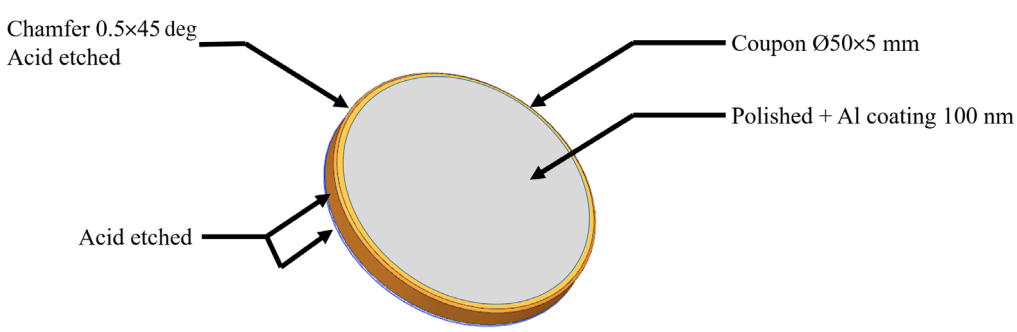

Fig. 8 ZERODUR® coupons designed for the electron irradiation experiment allow precision measurements.

coupon under the same operating condition was similar, thus showing that the presence of the Al layer has a neglectable effect on the charge monitoring;

- With aluminum coating, there is no need to paint the backface of the coupons to avoid spurious front-side/back-side interferences during interferometry. Thus, flash-coated coupons do not have variable stress imposed by painting.

The aluminum coating is not expected to impact the interpretation of the compaction results. Any possible changes in the optical figure introduced by the Al coating will be zeroed through the subtraction of the interferograms made after and prior irradiations on the same samples. The shielding of ZERODUR® introduced by the Al coating for the e^- energies considered in this text is insignificant; this statement has been numerically tested with MULASSIS[24] and can be straightforwardly be estimated by comparing the shield thickness $\delta = t * \rho$ (with penetration range t, density ρ) of the Al coating $\delta_{\mathrm{Al}} \simeq 1.2 \times 10^{-5} \times 2.70 = 3.2410^{-5}$ g.cm^{-2} with the ZERODUR® material $\delta_{\mathrm{ZERODUR®}} \simeq 0.25 \times 2.53 = 6.33 \times 10^{-1}$ g.cm^{-2}. It can also be argued that during the irradiation the Al coating may not be subject to compaction and that the coating will then counterbalance the effect of the ZERODUR® compaction, a first-order analysis of the bimetallic equation[19] demonstrates that this effect can only be marginal.

$$\frac{1}{R} = \frac{6(\epsilon_{\mathrm{Al}} - \epsilon_{\mathrm{ZERODUR®}})(1+m)^2}{h\left(3(1+m)^2 + (1+mn)\left(m^2 + \frac{1}{mn}\right)\right)} \simeq \frac{6(\epsilon_{\mathrm{Al}} - \epsilon_{\mathrm{ZERODUR®}})mn}{h}, \tag{8}$$

where R is the VRoC, ϵ is the linear strain, m the ratio of the thickness ($m = 120 \times 10^{-6}/5 \times 10^{0} = 2.4 \times 10^{-5}$), and n is the ratio of the Young modulus. Following this analysis, the strain induced by the aluminum coating should be about $10^4 - 10^5$ larger than the ZERODUR® strain to influence the shape of the sample.

Computational estimation due to the mechanical stress field is made using the Bourrieau-Romero compaction law[15] that suggested that local stress between 13 to 80 MPa could be expected in the material for high deposited dose, especially close to the edges of the discs. To prevent breakage due to this stress we acid etched the sidewall and backface of the blanks prior to the polishing. This etching suppresses subsurface damage resulting from machining with fixed abrasives and proved to significantly increase the bending strength, see Hartmann et al.[34] To ensure reregistration at before and after metrology, all coupons have clocking fiducial. The coupons were fixed on a dedicated metallic mount, having a hollow where the ZERODUR® discs fit. The coupons are maintained in the cavity by means of a metallic retaining ring covering the first 1 to $\in 2$ mm of the outer edge of the optical surface. This ring shields the coupon only over a minimal area taken into account in analysis.[35]

2.2.3 *Measure*

Consistant measurement of the coupons was done solely by Martin Valente at Arizona Optical System to avoid any difference between measurements before and after irradiation. The instrument used to measure the coupons is a Fizeau interferometer that uses polarization based phaseshifting to provide vibration insensitivity. The interferometer was positioned in a vertical downward looking orientation above the coupons. The coupons were mounted in the Faraday cup provided by Schott, and a kinematic three-point mount was used to support the coupons for the measurements. The interferometer was kept constant in calibration and configuration between the before and after measurements and temperature was carefully controlled. The coupons and the kinematic three-point mount were clocked relative to a reference scribe on the Faraday cup to match the mounting before and after registration for the measurements. Thus measured changes with the interferometer cannot be attributed to interforemeter systematic errors. To suppress any boundary effects caused by the metal ring during the irradiation we introduced an interferometric mask with a $\varnothing = 44$ mm aperture. The interferometer uses IntelliWave,[36] a commercial software package, to acquire and analyze the data. The measurement worksheets for the coupons (pre- and post-irradiation) were produced by a script that performed the following.

- Eight measurements were taken in quick succession and averaged together to create a data set;
- This process was performed eight times, producing eight data sets (each set is the average of eight individual measurements);
- The eight datasets were then averaged together to create a file for analysis.
- The interferometer error was calibrated out using a reference flat measurement. This error was subtracted from each of the coupon measurement files, for both pre- and post-irradiation cases;
- The pre-irradiation data set for each coupon was subtracted from the post-irradiation data set to determine the shape change caused by the radiation exposure.

Each of the following worksheets provides a contour map that represents the change in the coupon as a result of the exposure. The Zernike definition presented in each worksheet is based on the Optical Society of America standard definition.[37]

The reproductibility of the results has been tested on a non-irradiated control coupon that exhibited a deviation of −3.1 nm of the focus Zernike term, prior and after the irradiation campaign. Moreover, using the subsets of equally irradiated data it has been possible to calculate an average as well as standard deviation of the different Zernike coefficients. These statistical quantities are been reported on the figure provided in Sec. 2.2.5.

2.2.4 *Simulation*

The dose depth profile within a $\varnothing = 50$ mm, thickness 5-mm ZERODUR® disc calculated using Geant4[22,23] and is represented on Fig. 9. This profile corresponds to the dose deposited by a 1×10^{12} e − .cm^{-2} electronic charge in ZERODUR®. This computed dose profile has been weigthed by the different fluence experimentally tested, see Sec. 2.2.5. The radial dose distribution has also be extracted, it has been numerically possible to reproduce a normal radial dose distribution; however, the distribution is narrower with a σ parameter of $\sigma = 49.7$ mm, i.e., a deviation of about 12% from the experimental measure.

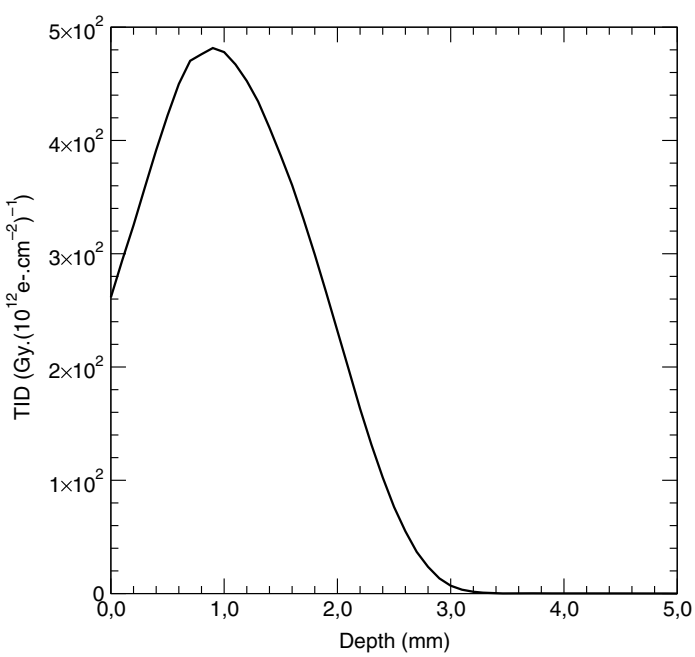

Fig. 9 Dose depth (TID) from e− is estimated using Geant4 corresponding to 1×10^{12} e − .cm^{-2} charge deposited over the ZERODUR® discs. The incident kinetic energy of the e− is $E = 1.5$ MeV.

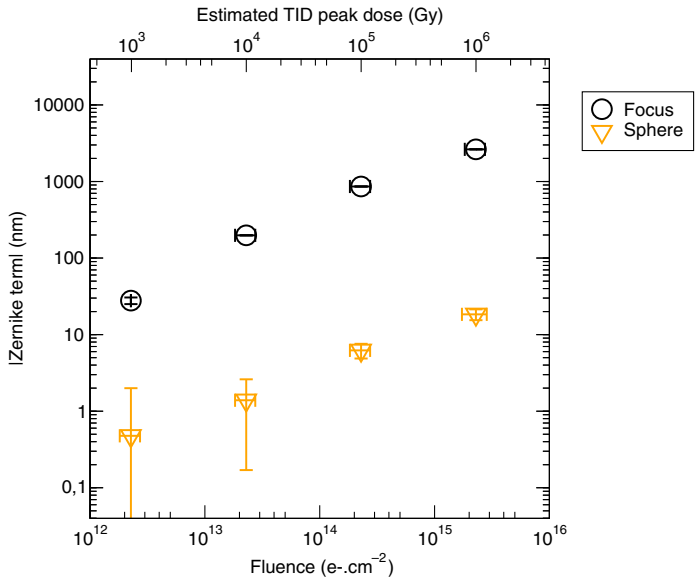

Fig. 10 Representation of the different absolute values of focus and sphere Zernike contributions represented as a function of the electronic fluence experimentally monitored (lower abscissa) also given as a function of the estimated TID (upper abscissa). The contribution of the focus term (circles) is clearly dominant on this plot.

2.2.5 *Results*

The axisymmetric dose imparted into the ZERODUR® discs results in a subsequent local compaction gradient that imparts in a pure spherical deformation of the coupons. This spherical deformation can be isolated by monitoring the focus Zernike term. A graphical representation of the absolute values of the first Zernike decomposition is provided in Fig. 10 where the preeminence of the focus term is clearly visible. Similar to the densities characterized over the γ irradiation experiments, we can directly observe that the focus Zernike coefficient can be described using a power-law regression. As expected, additional measurements made one year after the initial irradiations demonstrate that the surface errors recorded did not change substantially over this timespan.

2.3 *Proton Irradiation*

The measurement and irradiation procedure used with protons is basically the same as described in Sec. 2.2 for electrons.

2.3.1 *Irradiation configuration*

Proton irradiations has been carried out at the Compact Cyclotron via the commercial Zyklotron AG located at the Campus North of the Karlsruhe Institute of Technology (KIT). Negatively charged H^- hydrides are accelerated up to a fixed kinetic energy of about 25.3 MeV. The flux of H^- has its electron stripped at a metallic foil, the current of e^- ejected is then being used to indirectly monitor the flux of H^+ (typically with a $\pm 15\%$ precision) reaching the targets at an energy of about 23 MeV. At this energy the radial normal distribution profile of the particles on the target has a typical full-width at half-maximum (FWHM) close to 7 mm, which is far smaller than the diameter of the coupons. To achieve homogeneous irradiation, the coupons are assembled by means of Kapton® tape onto an XY mount (Fig. 11), Kapton® is prefered in this context as its adhesive properties holds over the irradiations runs. The coupons are raster scanned with respect to the beam spot to provide a uniform particle fluence over the entire coupon area.[38] The proton fluence is also cross monitored by means of the spectroscopy of activated nickel foils. The experiments were intentionally designed to have similarities to the γ and e^- irradiations

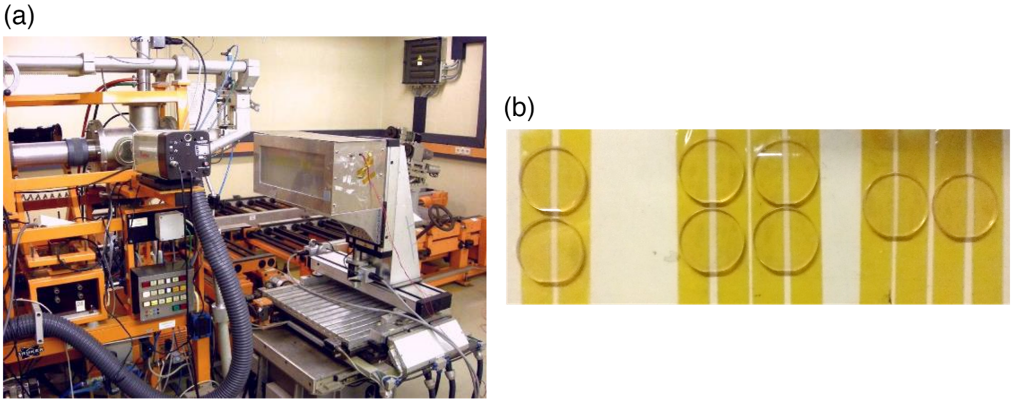

Fig. 11 (a) H^+ irradiation facility and (b) ZERODUR® coupons fixed on the XY mount made of Kapton®.

cases, and the overall TID was modulated over orders of magnitude while keeping the irradiation setup (positioning, incident particle energy, etc.) constant *via* modifying either the flux or the fluence. In this series increments in multiples ($10^n\times$) of the typical achievable fluence (3.4×10^{14} p.cm^{-2}) have been targeted. With this fluence, the TID close to ZERODUR® surface has been estimated at about 10^6 Gy. This energy deposited by the protons is converted into both ionization defects and a calorific contribution. In order to mitigate at best the competing thermally activated healing process, the average temperature of the coupons has been kept to 20°C by means of a N_2 air flux. However, the energy, the width of the proton spot (1.0 to 2.0 cm^{-2}) and the typical current of protons (about 2.0 μA) used in the scope of this experiment drove our design to a local moving spot with about 2.0 μA $\times$ 23 MeV = 46 W. With this setup, it is not possible to guarantee a perfectly homogeneous temperature field over the irradiation process. Previous experiments made on silicon at KIT suggested that local overheatings of $\Delta T \simeq +20$°C was observed under active cooling. This local reheating however is below the typical threshold ($T \geq 150$°C) observed by means of thermoluminescence measurements made on γ irradiated ZERODUR®. The high kinetic energy of the protons induced nuclear reaction within the ZERODUR® that activated the material. For safety reasons it was compulsory to let first the material decay (at least months) accordingly to German legislation prior to any interferometric measures.

The irradiation procedure has been repeated to gain statistical confidence, however, for practical reasons it has not been possible to equally repeat all the irradiations (in total we performed 2×10^7 Gy, 4×10^6 Gy, 4×10^5 Gy, and 2×10^3 Gy irradiations for a total of 12 coupons).

2.3.2 *Coupon design*

As with electrons, protons have a relative low penetration depth (large cross section compared to γ radiation) and also, similar to e$^-$, the characterization of the deformation can be better achieved by means of interferometry. The previous experiments carried out with electron irradiation (see Sec. 2.2), provide insight regarding the expected magnitude of the radiation induced deformations. With this information it was decided to refine the design toward the required metrology accuracy level, i.e., it is not necessary for the edges and back surface of the coupons to be acid etched nor the optical surfaces coated (see Sec. 2.2.2 for more comparitive details). ZERODUR® discs have been manufactured using standard double-side lapping and polishing processes, typically yielding the flatness of the coupons obtained to better than 1 μm RMS and the microroughness below 1 nm RMS. A fiducial clocking system has been introduced by machining a small feature (see Fig. 12). All the coupons have been prior measured interferometrically after polishing and prior to irradiation. As with electrons, the same metrological procedure and setup has been followed for the coupons measured after irradiation including precise registration of each coupons.

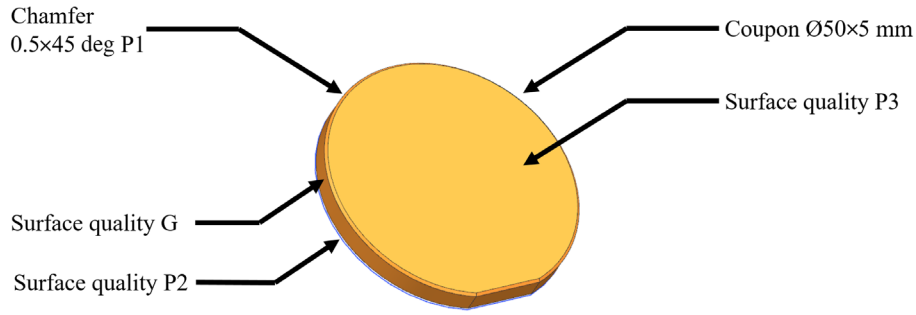

Fig. 12 ZERODUR® coupons designed for the proton irradiation experiment.

2.3.3 *Measure*

The coupons have been interferometrically measured both prior and after the irradiation. Based on the e- observation, see Sec. 2.2.3, we came to the conclusion that the effect of the gravitation on the optical figures of vertically standing coupons is negligible compared to the anticipated effect of proton ionization. For these measurements, the coupon were supported solely on their plano face, ensuring an optimal but simple clocking. The instrument used to measure the coupons is a 4-inch Zygo Verifire XPZ with a beam expander from 4 to 6 inches. This instrument uses polarization based phase-shifting to be relatively insensitive to vibrations. The interferometer environment is a room with temperature stabilization at $T = 21.5°\mathrm{C} \pm 5°\mathrm{C}$ on an air flotation optical table for vibration isolation. A closable plexiglass box suppresses air fluctuations. The stated specification of the equipment precision is $\lambda/20$ at HeNe (632.8 nm). However, calibrations have shown that this apparatus has an accuracy several times better than that. Each coupon has a serial number and an arrow on the edge which allows for precise reproduction of the positioning in a three-point mount. Mounting and measurement conditions are identical before and after irradiation. The interferometer uses commercial software termed "MX" that is provided by the manufacturer of the interferometer to acquire and analyze single measurements. The coupons have a diameter of 50 mm and the masking is for a clear aperture of 45 mm (with the exception of the 10^7 Gy case whose deformations were above the saturation level of the interferometer; in this case, we used a 25-mm aperture mask). The pre-irradiation data for each coupon is subtracted from the post-irradiation data to determine the shape change caused by the radiation exposure. For the analysis of the evolution between before and after irradiation, masking, translation corrections, and Zernike polynomial development a software is used called "scratch pad analysis" by the magneto rheological finishing (MRF) machine manufacturer QED Technologies.

The reproductibility of the results has been tested on a non-irradiated control coupon that exhibited a deviation of 3.42 nm of the focus Zernike term, prior to and after the irradiation campaign. Moreover, using the subsets of equally irradiated data it has been possible to calculate an average as well as standard deviation of the different Zernike coefficients. These statistical quantities are been reported in the figure provided in Sec. 2.3.5.

2.3.4 *Simulation*

The TID deposited in the ZERODUR® proton irradiation coupons is also estimated using Geant4.[22,23] In these simulations, the experimental XY stepwise advancing mount exposure, we substitute as an approximation a large collimated proton flux from normal to the surface of the coupon. The corresponding estimated ionizing dose deposition profile is represented on Fig. 13, a profile typical of Bragg curve with a Bragg peak located at half depth of the ZERODUR® coupons.

2.3.5 *Results*

The interferometric surface data corresponding to proton irradiation are very similar to those previously presented with electron doses (see Sec. 2.2.5), see Fig. 14. As expected, focus clearly

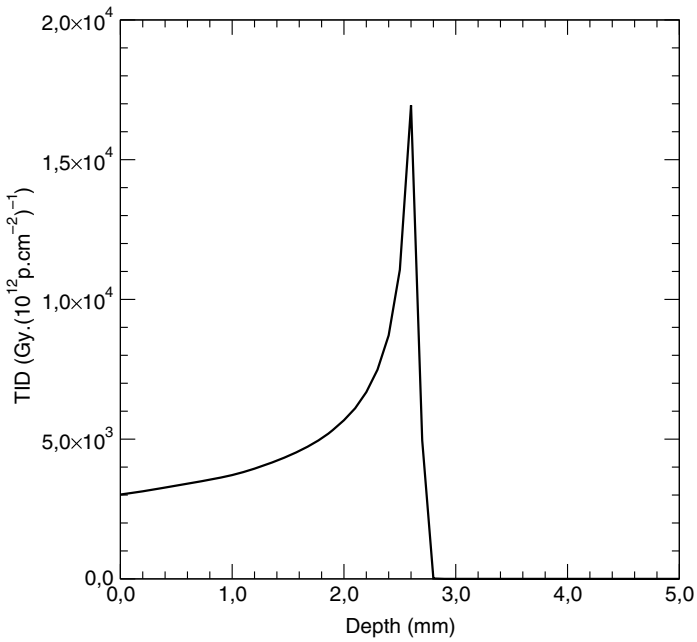

Fig. 13 Proton dose depth (TID) estimated using Geant4 corresponding to 1×10^{12} p.cm^{-2} charge deposited over the ZERODUR® discs. The incident kinetic energy of the H^+ is $E = 23$ MeV.

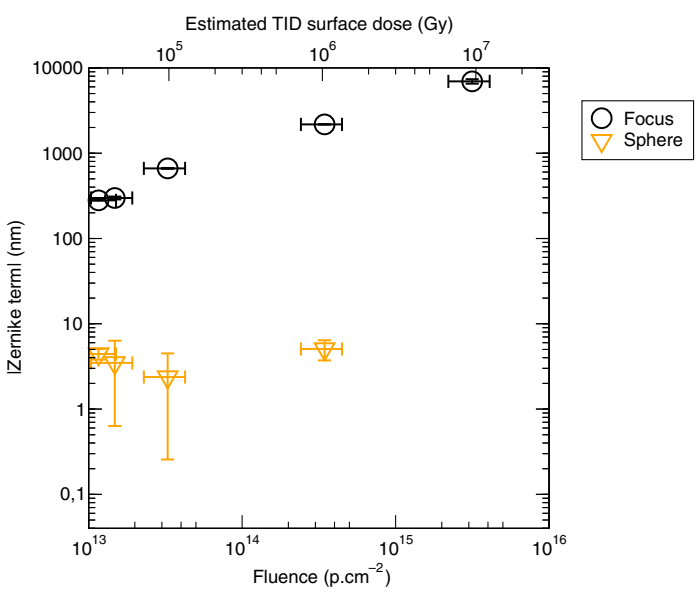

Fig. 14 Distribution of absolute Zernike contributions represented as a function of the experimentally monitored proton fluence. The seconday abscissa (top) represents the estimated TID surface dose deposited in the coupon derived from Monte Carlo method. The contribution of the focus term (circles) is also clearly dominant on this plot. The coupon deformation induced by the highest fluence tested required a narrowing of the interferometric mask (radius $r_{\text{small}}^{\text{mask}}$), the corresponding Zernike term can be corrected by means of a $(r_{\text{large}}^{\text{mask}}/r_{\text{small}}^{\text{mask}})^2$. This compensation has been introduced in this graphic to enable the comparison of the focus terms over the whole fluence tested but not for the other terms.

dominates the Zernike decomposition, and we observe a power law trend associating the focus term with the deposited dose.

3 Phenomenological Compaction Law

Derivation of a phenomenological compaction law based on the interferometric data is presented in the following subsections. First, the mathematical formulation chosen for the empirical compaction law will be presented. Choice in the selection of the experimental observables is explained. Then, coupled FEM/least square approach expanded in detail. Finally the results are summarized and compared with the literature data and spaceborne experience.

3.1 *Mathematical Model*

We assume the original power law model[15–17]

$$\Delta\rho/\rho(D) = A \times D^B. \tag{9}$$

This formulation presents both advantages and drawbacks. The experimental data gathered over the last forty years shows that a power law dependency reasonably describes the compaction phenomena. Moreover, the power law expression correctly assumes that there is no compaction without irradiation ($\Delta\rho/\rho(0) = 0$). Provided that the phenomenology of the compaction follows a power law of the imparted dose, it is then possible to determine independently the value of the exponent B from the value of the factor A. This is a direct scale invariance property of homogeneous functions.

In all the previous experiments the only experimental variable introduced adjust the amplitude of the TID profile within the coupon *via* the duration of irradiation exposure t, see Eq. (4). The dose-depth profile $D(z, t_1)$ expected for any arbitrary exposure time t_1 then can be inferred from an initial characterized dose deposition profile corresponding to an exposure time t_0 or from any given dose rate $\dot{D}(z)$

$$D(z, t_1) = \frac{t_1}{t_0} D(z, t_0) = t_1 \dot{D}(z). \tag{10}$$

Uncertainty may be assessed as follows: assume the observable X that varies with the variation of the density $X = g(\Delta\rho/\rho)$. Evoking a linear operator (e.g., $g: x \to x$ for X carrying the density variations $X(\Delta\rho/\rho(D)) = \Delta\rho/\rho(D)$, or integration $g: (x, u) \to \int_0^u x(z)\mathrm{d}z$ for X being the VRoC, i.e., $X \propto \int(\Delta\rho/\rho(D(z)))z\mathrm{d}z$[39]). Assuming a power law description of TID-induced strain ($\Delta\rho/\rho = A \times D^B$) directly defines that the observable X is an homogeneous function of the irradiation exposure time t. Mathematically $X_t = g(t\dot{D}) = t^B g(\dot{D})$. If we now introduce the compaction itself, we have

$$\Delta\rho/\rho(t_1\dot{D})/\Delta\rho/\rho(t_0\dot{D}) = (t_1/t_0)^B. \tag{11}$$

From Eq. (11) we can directly see that the exponent B is clearly accessible separately from A. The experimental observables as well as the exposure time (or equivalently the fluence), have been thoroughly monitored all over the experiments, enabling a straightforward determination of the validity of the power law. Thus, now the exponent B may be evaluated. The drawback in the power law formulation is that the compaction cannot be a monotonically increasing function of the dose and the density must reach limit. Because of this the power-law compaction should be used with special care and ideally only for interpolation purposes.

3.2 *Observables*

In the case of small spherical deformations on the coupon surface closed form relations bind the sagitta (sag), the peak-to-valley (PV), the Zernike focus coefficients, the optical power as well as the VRoC (R). These relations are derived from the Zernike coefficients definition

$$a_{l,n} = \frac{2n+2}{\epsilon_l \pi} \int_{\phi=0}^{2\pi} \int_{\rho=0}^{\rho=1} G(\rho,\phi) * Z_n^l(\rho,\phi) \rho \mathrm{d}\rho \, \mathrm{d}\phi, \tag{12}$$

where ρ in this specific context describes the normed radial distance (and in this case not the density), ϕ the azimuthal angle, and ϵ_m the Neumann factor defined as 2 if $m = 0$ and 1 if $m \neq 0$. The function $G(\rho,\phi)$ describes the local height of the coupon surface in cylindrical coordinates. The Zernike focus term corresponds to the $l = 0$ and $n = 2$ contribution mathematically defined

$$a_{0,2} = \frac{3}{\pi} \int_{\phi=0}^{2\pi} \int_{\rho=0}^{\rho=1} G(\rho,\phi) * (2\rho^2 - 1) \rho \mathrm{d}\rho \, \mathrm{d}\phi. \tag{13}$$

Here we find the experimental Zernike focus contribution to be the more significant term, i.e. the coupons deformation is dominated by a spherical contribution. Although a dominant response term, this deformation remains small compared to the large optically generated radius of curvature of our coupons r. Thus, we approximate the irradiation induced deformation $G(\rho,\phi)$ by a first order Taylor expansion of the spherical deformation

$$G(\rho,\phi) = R - R\sqrt{\left(1 - \left(\frac{\rho r}{R}\right)^2\right)} \simeq \frac{(\rho r)^2}{2R^2} \quad \text{for } \frac{\rho r}{R} \simeq 0, \quad \text{i.e., } r \ll R. \tag{14}$$

Using the above expression, we can easily estimate the PV value

$$PV = G(\rho = 1) - G(\rho = 0) = \frac{1}{2}\frac{r^2}{R}. \tag{15}$$

If we now combine Eqs. (13) and (14) we obtain

$$a_{0,2} = \frac{1}{4}\frac{r^2}{R}. \tag{16}$$

Due to a pure spherical deformation, the $a_{0,2}$ coefficient scales like the half of PV, which corresponds also to the definition of the optical sagitta $a_{0,2} = PV/2 = \mathrm{sag}/2$. While either the measured PV or measured Sagitta (Sag) can be used to estimate the curvature of the coupons the PV estimation can be biased by local surface imperfections. Thus we preferred using the more robust focus term, in the following section Sec. 3.3 the sagitta deformation is defined $\mathrm{sag} = 2a_{0,2}$. Note that we calculated this sagitta for a $r = 25$ mm diameter by rescaling the defocus term by a factor $(r/r_{\mathrm{aperture}})^2$ to correct for the truncation introduced by the interferometric masks.

3.3 *Numerical Fit*

The compaction law driving to the defocuses observed for different maximal peak doses can be inferred numerically iteratively guessing the factor A and exponent B of the power law describing the empirical compaction law binding the compaction to the local deposited dose $\Delta\rho/\rho = A \times D^B$. To this end, a Nelder-Mead χ^2 minimization procedure[40,41] has been implemented, the cost function has been defined

$$\chi^2(\{A;B\}) = \sum_{i \in \{10^2,\ldots,10^6\}\ \mathrm{Gy}} (\mathrm{sag}_i^{\mathrm{exp.}} - \mathrm{sag}_i^{\mathrm{sim.}}(\{A;B\}))^2, \tag{17}$$

where $\mathrm{sag}_i^{\mathrm{exp.}} = 2a_{0,2}^{\mathrm{exp.}}$. represents the average sagitta experimentally derived from the defocus terms corresponding to the estimated dose peak i.

The $\mathrm{sag}_i^{\mathrm{sim.}}$ represent the sagitta calculated by means of FEM solution using the $\{A;B\}$ parameter set. Over the numerical iteration processes, the local dose field per FEM nodes is converted into a strain field (via the iteratively guessed phenomenological compaction law) and then into a stress field. The FEM solution calculates the deformations that minimize the

stress-field. Next, these deformations are compared with the experimental values through the χ^2. The dose distribution is assumed to follow a normal radial distribution for the electrons $\sigma = 58.3$ mm and a flat distribution for the protons. Note while the least-square procedure could have been performed using a one dimensional continuous Timoschenko model,[39] such an approach would require further simplifications (radial homogeneity of the dose distribution, thin plate approximation, low deformations), the validity of which we question (see again Davis and Fainberg[14]). This alternative numerical procedure translates experimentally observed surface deformation (the only matter of importance for the optical designer) into density variations via a non-linear fitting scheme. However, the error bars relative to the deformation measurements cannot be directly converted and graphically plotted onto the compaction diagram.

3.4 *FEM Simulations*

The ABAQUS[42] FEM software has been used for the simulation of the deformation of ZERODUR® $\phi = 50$ mm thickness $= 5$ mm coupons. The system has been computed assuming a rotationally symmetrical 2D model appropriate to the nature of the deformation observed on the coupons, see Fig. 15. The meshing is a made using a rectangular pattern, the element size being 0.1 mm long and 0.05 mm thick. The overall simulation domain is composed of ≃25000 of these cells. The preprocessing of the geometry and of the mesh has been achieved using the CUBIT and Coreform Trelis solution. The central node located at the intersection of the backface and the rotation symmetry axis is fixed, while all other nodes were unconstrained.

The system relaxation has been computed using the temperature solver of ABAQUS, where we substituted at first order the thermal strain $\epsilon = \Delta l/l(T)$ by the compaction $\epsilon \propto \Delta\rho/\rho(D)$. The expression of strain $\Delta l/l$ can be derived from the compaction by considering a small

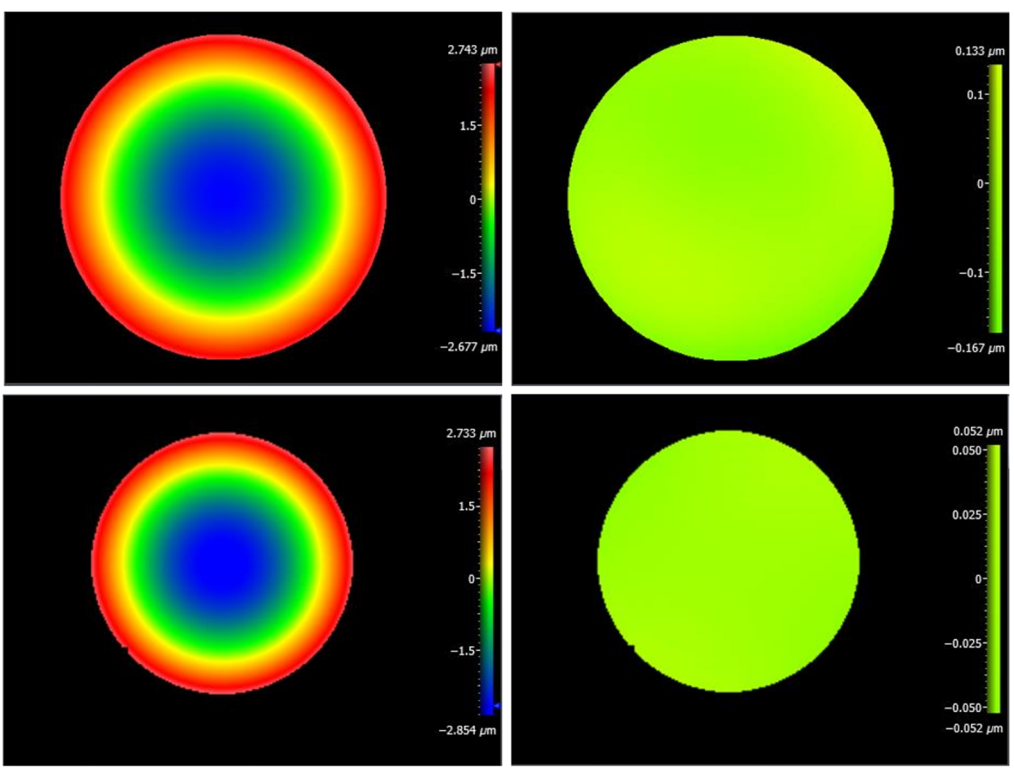

Fig. 15 Synthetic interferograms generated by subtracting the surface of the coupon after and from prior irradiation. Top: electron irradiation. Bottom: proton irradiation. (Since the deformation was too large at the edges for this scaling we introduced an edge mask.) Left: surface without contribution of tilt and piston. Right: surface without contribution of tilt, piston, and defocus (power). The color scaling has been kept constant to support the left/right comparison. The Zernike focus contribution to the deformation is in both cases clearly by far the dominant one.

isotropic cubic control volume of edge length l containing a mass m having a density $\rho = m/l^3$. Based on this formalism we have

$$l = l_0\left(1 + \frac{\Delta\rho}{\rho}\right)^{-\frac{1}{3}}. \tag{18}$$

And for relatively small variations of density ($\Delta\rho/\rho \ll 1$), we can approximate the above expression by a first order Taylor expansion of the compaction

$$l \simeq l_0\left(1 - \frac{1}{3}\frac{\Delta\rho}{\rho}\right), \tag{19}$$

consequently:

$$\epsilon = \frac{\Delta l}{l} \simeq -\frac{1}{3}\frac{\Delta\rho}{\rho}. \tag{20}$$

Based on the above expression, we can see that a direct analogy can be drawn with the linear thermal strain.

A 2D cross section of the simulation area prior and after mechanical relaxation is illustrated on Fig. 16.

3.5 *Discussion*

In preamble to this discussion, we summarized on Table 3 the different prior estimations of ZERODUR® density compaction law expressed for TID in Gray. Unfortunately, some of the data are not accessible as via the corresponding publications due to typo errors. In her work, Higby[16] substituted the prefactor A in Eq. (9) with $A := \log_{10} A$. Because of this, readers may conclude that the compaction prefactor proposed in Higby[16] is $A = -4.52$ from following her formalism though we may infer that proposed by Higby reads now $A = 10^{-4.52-2+2*0.38} = 1.74 \times 10^{-6}$, see Ref. 44 where the -2 corresponds to the conversion from percent compaction into compaction, the $+2 * 0.38$ corresponds to the conversion unit between rad and Gray and 0.38 corresponds to the exponent proposed in Ref. 16. It is worthwhile to mention these details, even though the exact same confusion can be read in Edwards et al.,[18] where an additional misinterpretation between natural logarithm ln and the $\log_{10}$ function used in Ref. 16 has been introduced.

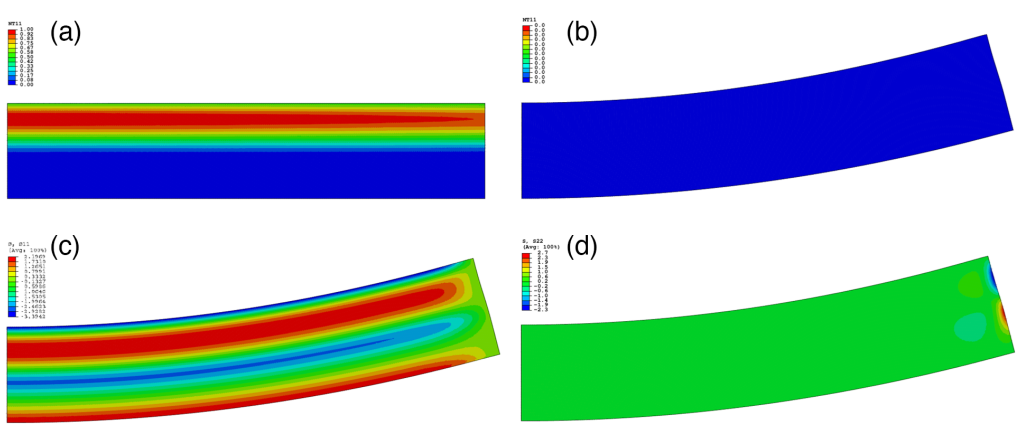

Fig. 16 Axial symmetric 2D radial cross sections of a simulated ZERODUR® coupon corresponding to a electronic TID peak of 10^6 Gy. The deformations (both axial and radial) have been magnified by a factor 500×. (a) Strain field (normalized), (b) strain field after mechanical relaxation, (c) mechanical stress field (axial), and (d) mechanical stress field (radial). On panel (c), the compacted area applies a tensile stress on the surrounding material, the disc bends. Meanwhile, the convex stretched back face of the disc applies also a counteracting tensile stress.

Table 3 List of density compaction laws for TID doses (D) in gray $\Delta\rho/\rho = \mathrm{AD}^B$ proposed by different authors.

Authors	Particles	Prefactor (A)	Exponent (B)
Bourrieau and Romero[14,15,25]	e^-, H^+	9.0×10^{-7}	0.50
Higby et al.[16]	e^-	1.74×10^{-6}	0.38
Davis and Fainberg[14]	e^-, H^+	0.75×10^{-7}	0.50
Edwards et al.[18]	H^+	—	0.194 – 0.53
Rajaram et al.[43]	e^-	—	0.37
This publication	e^-	2.39×10^{-7}	0.51
This publication	H^+	0.97×10^{-7}	0.53

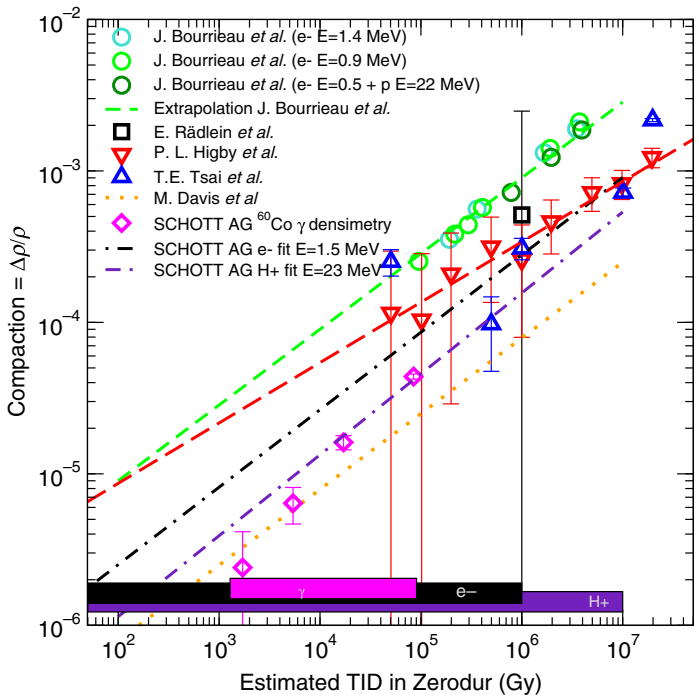

Fig. 17 Collection of phenomenological density compaction laws. Green/circles and dashed line: Bourrieau and Romero[15] contribution (TID estimated for ZERODUR®). Red/triangle down: Higby et al.[16] contribution (TID measured in Si). Blue/triangle up: Tsai et al.[17] contribution (TID given for unspecified material). Magenta/diamonds: Schott compaction law determined on ^{60}Co (TID estimated for ZERODUR®). Black/dash-dotted line: Schott compaction law determined using e^- (TID estimated for ZERODUR®). Violet/dash-dash-dotted line: Schott compaction law determined for H^+ (TID estimated for ZERODUR®). Orange/dotted line: reassessement of Bourrieau et al.[15] proposed by Davis and Fainberg.[14]

Our new compaction laws, as well as the γ compaction law, have been superimposed on selected data available in the literature; see Fig. 17.

Regarding the e^- irradiation, the new phenomenological compaction diverges significantly from that of Bourriau and Romero.[15] As experienced by Davis and Fainberg[14] the compaction assumed by Bourrieau and Romero[15] significantly overestimates the experimental compaction observations. This overestimation is, however, not as large as initially suggested by Davis,[14] who proposes a rescaling of the prefactor of about 1/12 based on physical considerations

(i.e., $A_{\text{Davis}} = A_{\text{Bourrieau}}/12 = 9.0/12 \times 10^{-7} = 0.75 \times 10^{-7}$), but is still in agreement with their simulation results, which drove the authors[14] to estimate the compaction prefactor being 5× to 10× lower than the first estimate made by Bourrieau and Romero.[15] The equivalent TID D_{eq} necessary to achieve the same level of compaction using the Bourrieau and the compaction law proposed in this study can be derived as follows:

$$\left.\frac{\Delta\rho}{\rho}\right|_{\text{BR}} = 9.0 \times 10^{-7} D^{0.5} = 2.39 \times 10^{-7} D_{\text{eq}}^{0.5} = \left.\frac{\Delta\rho}{\rho}\right|_{\text{present study}}, \tag{21}$$

$$D = \left(\frac{2.39}{9.0}\right)^2 D_{\text{eq}}, \tag{22}$$

$$9.0 \times 10^{-7} D^{0.5} = 9.0 \times 10^{-7} \left(\left(\frac{2.39}{9.0}\right)^2 D_{\text{eq}}\right)^{0.5}, \tag{23}$$

$$D = 0.0705 D_{\text{eq}}. \tag{24}$$

This study supports that the level of TID necessary to induce a given level of compaction was underestimated by a factor $1/0.0705 \simeq 14$ with the Bourrieau[15] compaction law. Thus ZERODUR® is less sensitive to ionizing radiation than suggested by prior studies.

For a high electron dose (i.e., around 10^6 Gy) we can see that the Higby[16] data and the present compaction law derived for electron match reasonably well. For lower deposited ionizing dose (<10^5 Gy) we can see that the experimental data measured in Ref. 16 are systematically above the electronic compaction law proposed here. These experimental data points affected the regression fit proposed in this work (red-dashed line in Fig. 17). This effect is probably due to the earlier difficulty of measuring the compaction by means of density gradient column at this level. As a consequence, the exponent value of the power law regression is lower and therefore the compaction for lower doses was assumed being higher.

Similar to electrons we see that the proton compaction law proposed in this work also has an exponent close to 0.5 though with a very different prefactor. This observation is in clear disagreement with the study of Bourrieau and Romero,[15] who suggest that electrons as well as protons (irrespective of their kinetic energies) are inducing the exact same compaction.

However, we observe one order of magnitude between this present and past phenomenological law. It follows that ZERODUR®'s response to radiation is an order of magnitude lower than would be predicted by earlier compaction laws and far more relevant to actual experience in space. Our compaction law also finds a by far lower compaction level compared to the Bourrieau and Romero work.[15]

The γ compaction law is also assuming a far lower compaction level compared to the Bourriau and Romero work.[15] Over their overlapping ionizing dose-domains the γ and protonic compaction law derived in this work are in a fairly good agreement.

4 Conclusion

We proposed to shed light on the behavior of ZERODUR® under typical spaceborne ionizing radiations levels, especially in the context of no reported compaction changes in over 30 spaceborne missions. Specifically, we focused on the material shrinkage under γ, e^-, and H^+ radiations. To this end the material deformation was investigated using two main measurement pathes, one based on the direct measurement of the density changes (adapted for penetrating radiation, such as γ) and the other one based on the characterization of the deformation (adapted for low penetrating radiations, such as e^- and H^+). These two approaches confirmed that the compaction of ZERODUR® can be qualitatively well be described by power-law phenomenological formulation related to the estimated TID. By coupling these experimental results with FEM approaches, we have confirmed the first intuition of Davis and Fainberg[14] stating that the prior compaction published to date were significantly overestimating the compaction of ZERODUR® under most realistic levels of space ionizing radiation. We observed that all the compaction laws derived in this work are scaling similar to a square-root function of the

TID in qualitative agreement with previous works published on this subject. For mathematical and physical reasons, any optical deformations induced by radial homogeneous TID deposited on an optical substrate should follow this square-root scaling of the TID. Interestingly this trend has not been observed by Doyle et al.[25] during the irradiation of the SILEX replica mirrors[25] whose deformation were found to scale linearly with the absorbed dose (implying an exponent $B = 1$ in the compaction law, in systematic disagreement with all investigations made on ZERODUR® compaction so far). This mismatch calls for a reassessment of the SILEX data. Typically, the defects induced by ionizing radiation heal, if the damaging kinetic (typical time scale of the ionizing experiments) is faster than the healing kinetic of the material. Thus results monitored directly after irradiation may not be representative of the flight-state. Since the healing kinetic for ZERODUR® compaction is presently unknown, we cannot ensure that the specimens considered in this work were fully relaxed, a second series of measures on the electron and proton irradiated samples one year after the irradiation suggests that the deformations do not relax with time. Other sets of measures on the specimens presented in this work are scheduled to be within the next decade, i.e., typical time scale of standard space mission.

This study, conducted to accuracy levels, establishes that radiation response of ZERODUR® is at least an order of magnitude lower than prior compaction models. These prior models do not match the anecdotal evidence that in over 30 noted orbital missions, none report reduction of optical errors due to environmental radiation.[2,3] Thus, our revised models, demonstrating that for most orbital scenarios and mirror exposures very little compaction is expected, are far more consistent with decades of experience flying ZERODUR®.

The dose depth profile within a $\phi = 50$ mm, thickness 5-mm ZERODUR® disc, was calculated using Geant4[22,23] and is represented on Fig. 9. This profile corresponds to the dose deposited by a 1×10^{12} $e - cm^{-2}$ electronic charge in ZERODUR®. This computed dose profile has been weigthed by the different fluence experimentally tested, see Sec. 2.2.5. The radial dose distribution has also be extracted, it has been numerically possible to reproduce a normal radial dose distribution, however the distribution is narrower with a σ parameter of $\sigma = 49.7$ mm, i.e., a deviation of about 12% from the experimental measure.

Acknowledgments

The authors of this publication would like to thank Dominic Doyle (former ESA member) for his strong and steady support and inputs during this work, we would also like to thank Peter Hartmann for his valuable insights about ZERODUR®, Paige Higby for her interpretation of past published data and Mark Davis, who initially triggered this activity and guided us through this problem. This work would not have been possible without third institutions, namely the Institute of Experimental Particle Physics of the KIT as well as former member of Advanced Optical System for their inputs during the design of the coupons.

References

1. SCHOTT AG, "Brochures and downloads for ZERODUR® glass," 2013, https://www.schott.com/en-gb/products/zerodur-p1000269/downloads (accessed 18 April 2023).
2. T. Döhring et al., "Forty years of ZERODUR mirror substrates for astronomy: review and outlook," *Proc. SPIE* **7018**, 70183B (2008).
3. J. Krieg et al., "The past decade of ZERODUR glass-ceramics in space applications," *Proc. SPIE* **12180**, 121805N (2022).
4. H. Bach and D. Krause, *Low Thermal Expansion Glass Ceramics*, Springer (2005).
5. P. Hartmann et al., "Glass ceramic ZERODUR®: even closer to zero thermal expansion: a review, part 1," *J. Astron. Telesc. Instrum. Syst.* **7**(2), 020901 (2021).
6. P. Hartmann et al., "Glass ceramic ZERODUR®: even closer to zero thermal expansion: a review, part 2," *J. Astron. Telesc. Instrum. Syst.* **7**(2), 020902 (2021).
7. A. Carré et al., "Zerodur stability in space environments," *Proc. SPIE* **11852**, 118524S (2021).
8. R. E. Schenker and W. G. Oldham, "Ultraviolet-induced densification in fused silica," *J. Appl. Phys.* **82**(3), 1065–1071 (1997).

9. W. Primak and R. Kampwirth, "The radiation compaction of vitreous silica," *J. Appl. Phys.* **39**(12), 5651–5658 (1968).
10. E. J. Friebele and P. L. Higby, "Radiation effects in amorphous sio2 for windows and mirror substrates," in *Proc. Symp. Laser Induced Damage (NIST, Boulder CO, 1998)*, pp. 89–97 (1988).
11. C. B. Norris and E. P. EerNisse, "Ionization dilatation effects in fused silica from 2 to 18-kev electron irradiation," *J. Appl. Phys.* **45**(9), 3876–3882 (1974).
12. C. I. Merzbacher et al., "Finite element analysis of deformation in large optics due to space environment radiation," *Proc. SPIE* **1533**, 222–228 (1991).
13. J. E. Shelby, "Radiation effects in hydrogen-impregnated vitreous silica," *J. Appl. Phys.* **50**(5), 3702–3706 (1979).
14. M. J. Davis and J. Fainberg, "Compaction effects of radiation on Zerodur," *Proc. SPIE* **5179**, 38–49 (2003).
15. J. Bourrieau and M. Romero, "Effect of space charged particle environment on optical components and materials," in *ESA Spacecr. Mater. in Space Environ. (SEE N80-21420 12-23)*, pp. 275–285 (1979).
16. P. L. Higby et al., "Radiation effects on the physical properties of low-expansion-coefficient glasses and ceramics," *J. Am. Ceram. Soc.* **71**(9), 796–802 (1988).
17. T. E. Tsai et al., "Radiation effects on a low-thermal-expansion glass ceramic," *J. Appl. Phys.* **62**(8), 3488–3490 (1987).
18. D. L. Edwards et al., "Investigation into radiation-induced compaction of ZERODUR® TM," NASA Technical Memorandum 108505 (1996).
19. S. Timoshenko, "Analysis of bi-metal thermostats," *Journal of Optical Society of America* **11**, 233–255 (1925).
20. D. Doyle, Former Senior Scientist, ESA ESTEC TEC-MMO, private communication.
21. A. Carré et al., "Resilience of ZERODUR glass ceramic under ionizing radiations," *Proc. SPIE* **12188**, 1218805 (2022).
22. J. Allison et al., "Recent developments in geant4," *Nucl. Instrum. Methods Phys. Res., Sect. A* **835**, 186–225 (2016).
23. S. Agostinelli et al., "Geant4—a simulation toolkit," *Nucl. Instrum. Methods Phys. Res., Sect. A* **506**(3), 250–303 (2003).
24. S. Clucas, "SPENVIS – space environments, effects and education system," Version 4.6.11, 26 August 2022, https://www.spenvis.oma.be/ (accessed 18 April 2023).
25. D. B. Doyle et al., "Effect of electron irradiation on the radius of curvature of a zerodur mirror," *Proc. SPIE* **2775**, 166–188 (1996).
26. A. Holmes-Siedle and L. Adams, *Handbook of Radiation Effects*, Oxford University Press, Inc., New York (1993).
27. A. Costantino and M. Muschitiello, "ESTEC Co-60 irradiation facility – 2018 uniformity of irradiation field verification," Technical Note, ESA-TECQEC-LAB-TN-008871 (21 March 2018).
28. H. Bettin et al., "Cleaning of silicon density standards," in *Proc. XIX IMEKO World Congr.*, Vol. 1, pp. 179–181 (2009).
29. M. Vogtmann, "Calibration certificate," Reference No. 1.82-2019A012, Calibration mark: PTB-11316 19, PTB Braunschweig (8 May 2019).
30. A. Costantino and M. Muschitiello, "Estimation of source self absorption coefficient after May 2016 source reload at ESTEC Co-60 irradiation," Technical Note, ESA-TECQEC-LAB-TN-002461 (2 June 2016).
31. S. M. Seltzer, "X-ray mass attenuation coefficients," National Institute of Standards and Technology, 17 February 2022, https://physics.nist.gov/PhysRefData/XrayMassCoef/tab4.html (accessed 18 April 2023).
32. A. Schüller et al., "Traceable charge measurement of the pulses of a 27 MeV electron beam from a linear accelerator," *J. Instrum.* **12**, P03003–P03003 (2017).
33. A. Bourgouin et al., "Characterization of the PTB ultra-high pulse dose rate reference electron beam," *Phys. Med. Biol.* **67**, 085013 (2022).
34. P. Hartmann et al., "Zerodur: bending strength data for etched surfaces," *Proc. SPIE* **9151**, 91512 (2014).

35. A. Carré et al., "An empirical approach for space-based mirrors to evaluate the extent of radiation compaction under expected environmental doses," *Proc. SPIE* **11852**, 118524U (2021).
36. B. Ionita et al., "Intelliwave interferometric analysis software in laser interferometry laboratory," *Proc. SPIE* **7297**, 232–237 (2009).
37. L. N. Thibos et al., "Standards for reporting the optical aberrations of eyes," *Journal of Refractive Surgery* **18**(5), S652–S660 (2002).
38. A. Dierlamm, "Studies on the radiation hardness of silicon sensors," PhD thesis, Universität Karlsruhe (TH), IEKP-KA/2003-23 (2003).
39. J. W. Pepi, *Opto-structural Analysis*, SPIE Press, Bellingham, Washington (2018).
40. F. Gao and L. Han, "Implementing the Nelder-Mead simplex algorithm with adaptive parameters," *Comput. Optim. Appl.* **51**(1), 259–277 (2012).
41. K. J. M. C. R. Harris et al., "Array programming with NumPy," *Nature* **585**, 357–362 (2020).
42. M. Smith, *ABAQUS/Standard User's Manual, Version 6.9*, Dassault Systèmes Simulia Corp., United States (2009).
43. M. Rajaram, T. Tsai, and E. J. Friebele, "Radiation-induced surface deformation in low-thermal-expansion glasses and glass-ceramics," *Adv. Ceram. Mater.* **3**(6), 598–600 (1988).
44. P. L. Higby, Senior Scientist, Schott North America former Member of Naval Research Laboratory, E-mail communication (16 December 2022).

Antoine Carré is working as a senior material scientist in the development department of the optic business unit of the Schott AG glass manufacturer. For more than 13 years at Schott, he has steadily supported the process optimization of the glass ceramic ZERODUR® and deepened our understanding of this material. Prior to his duty at Schott AG, he was part of a programming team developing a material microstructure simulation software mostly used for the description of metallic solidification process.

Rule Kirchhoff studied industrial furnace technology at TU Bergakademie Freiberg from 1986 to 1991. He then worked as a research assistant at the Institute for Heat Engineering of the TU BA Freiberg and at the Institute for Foundry and Metallurgical Technology at Gerhard-Mercator-Universität GH Duisburg. His work focused on the radiation properties of refractory materials. Since 1998, he has been a consultant for melting technology development and model application at Schott AG.

Tony Hull is working as an adjunct professor of physics and astronomy at the University of New Mexico and is in his fifth decade of being active developing space missions. He has served as director of program management at Perkin-Elmer AOD, vice president and chief scientist at Optical Corporation of America, principal engineer for observational systems at JPL, NASA's technologist for Terrestrial Planet Finder Coronagraph, and director over polishing the full suite of JWST mirrors. Recently, he has been an architect of CETUS, a NASA funded Probe Mission Study and presently is serving on NASA's COR Ultrastable Observatory Roadmap Team addressing HWO requirements. He consults extensively, including on ZERODUR® applications for Schott AG.

Janina Krieg received her PhD in material science in 2017 at TU Darmstadt and is working as a physicist. In her research field of nanotechnology, she worked with graphene and topological insulator materials. In 2022, she completed an executive MBA program from Mainz University. Since 2017, she has been the responsible product manager for ZERODUR® glass ceramics at SCHOTT AG, Mainz, with a focus on mirror substrates for space applications.

Daniela Eppers received her MSc and the Dr. rer. nat. degrees from Technische Universität Braunschweig, Germany, in 2010 and 2015. In 2014, she joined PTB Braunschweig, Germany, where she is engaged in the development of high precision density measuring methods for solids.

Marty Valente: Biography is not available.

Thomas Westerhoff, physicist by training, joined the Optics Business at Schott as product manager in 1996. He was promoted to director of sales and marketing Schott Lithotec in 1999. In 2007, he took responsibility for the Schott product group ZERODUR®. In 2018, he was promoted to the position vice president strategic business field ZERODUR® responsible for astronomy and space, IC and FPD lithography, and industrial application.